Use Authorization

In presenting this thesis in partial fulfillment of the requirements for an advanced degree at Idaho State University, I agree that the Library shall make it freely available for inspection. I further state that permission to download and/or print my thesis for scholarly purposes may be granted by the Dean of the Graduate School, Dean of my academic division, or by the University Librarian. It is understood that any copying or publication of this thesis for financial gain shall not be allowed without my written permission.

Signature _____

Harishchandra Aryal

Date _____

Small Reactivity Measurement in Advanced Test Reactor Critical (ATR-C) and Neutron Radiography (NRAD) Reactor and an Oscillator Design

By

Harishchandra Aryal

A thesis

Submitted in partial fulfillment

of the requirements for the degree of

Master of Science in Nuclear Science and Engineering

Idaho State University

Spring 2014

To the Graduate Faculty:

The members of the committee appointed to examine the thesis of Harishchandra Aryal find it satisfactory and recommend that it be accepted.

_____

Dr. George Imel,

Major Advisor

_____

Dr. Jason Harris,

Committee Member

_____

Dr. Marco P. Schoen,

Graduate Faculty Representative

ACKNOWLEDGEMENTS

Before beginning, it is my utmost honor to acknowledge the people who in one way or another contributed in completion of this thesis. I would not have been able to get it done without the support from my committee members, close friends and family.

A special thanks to my major advisor Dr. George Imel for his continual support throughout my thesis. His knowledge, patience and encouragement were crucial to the completion. I would like to thank Dr. Jason Harris for his help. I would like to express my deepest appreciation to all other professors who contributed.

I thank my friendly and cheerful fellow students of the research group especially to Ben Baker and Tony Riley for providing valuable insights throughout the work. I am grateful to all my friends mostly my girlfriend, Savyata Subedi for her unfailing support.

Words seem inadequate to describe the support my family has provided to come to this point. A billion thank you to my mom for helping me out when I needed. You probably assisted more than you think you did. I am always indebted to my dad for the care, patience and encouragement that had been shown towards me in completing this thesis. I could not forget my sister, Muna Aryal and brother-in-law, Binod Rizal for their corroborations. The time they spent and knowledge they shared were truly precious.

Table of Contents

List of Figures

List of Tables

ABSTRACT

This thesis presents a simple method of determining small reactivity using an open loop oscillator technique. This technique was initially proposed for Advanced Test Reactor-Critical (ATR-C) at Idaho National Laboratory. Later, it was found that ATR-C was not a good choice due to its complex geometry (clover-leaf) and its characteristic of having a tremendous coupling of the higher harmonics with the fundamental mode. However, an open loop method was found to be a valid and a precise method to measure small reactivity in simpler reactors like Neutron Radiography (NRAD) and AGN-201. For the convenience of the reader several plots such as: flux profile of the ATR-C core, 3 D plot of flux across ATR-C, plot with higher expansion coefficients of the ATR-C flux, transfer function plot of NRAD and its comparison with the ISU-AGN-201 reactor are also presented. After realizing the fact that this technique could be used in NRAD, a simple oscillator design is also presented in this thesis.

Chapter 1: INTRODUCTION

This thesis is a part of a larger project at Idaho State University (ISU). The project, as a whole, is about building an infrastructure for an open loop technique and implementing this technique to measure reactivity worth of small samples. Many closed loop systems have been already in practice that require an extra calibrating pilot rod and as a result adds complications and costs. If the open loop technique can give reactivity measurements with similar or better precision and accuracy, it could be a great benefit. Moreover, this can be installed on those facilities where more complex closed system cannot be incorporated easily.

Using the open loop technique, the transfer function of a reactor such as neutron radiography reactor (NRAD) can be computed. The magnitude of transfer function correlates the reactivity of the sample that caused the perturbation. In addition, the open loop transfer function allows one to determine whether the reactor is a stable system or not. In other words, the reactor's response to the change in neutron population in the reactor can be easily described. Moreover, a transfer function measurement is useful to extract important kinetic parameters of the reactor system, as for instance prompt neutron generation lifetime, reactivity shutdown margin, absolute power etc.

There are a few limitations in determining reactivity of small worth samples. The most important limitation is the reactor noise. Reactor noise is defined as the inherent fluctuation in neutron level due to the statistical distribution of fission neutrons. The origin of such fluctuations might be either mechanical or neutronic. Mechanical variations are caused by the movement of the control rods, coolant flow across the

channels, natural vibration of the system, etc. In zero power reactors, mechanical contribution to the reactor noise is negligible (Raines, 1971). On the other hand, neutronic fluctuation are caused due to the discrete nature of fission, capture, and leakage (Raines, 1971). A theoretical reactivity limit for reactivity measurement was calculated by Foell (Foell, 1972). For example,the variance of a U-235 fueled reactor such as NRAD is given as:

$$\sigma(t) = \frac{5.1}{\sqrt{Wt}} \times 10^{-6} \frac{\Delta k}{k} \quad [1]$$

Where, W is the reactor power in watts, t is the time of measurement in seconds and k is the multiplication factor. Equation 1 gives the minimum uncertainty that could be achieved from a reactor. It can be seen from equation 1 that uncertainty depends on two factors, t and W. Time of measurement could be shortened by operating at higher power but at higher power feedback effects such as temperature will interfere. Thus, a proper selection of time and power is crucial. As for instance, if NRAD is operated at a power of 50 watt for 100 second, $\sigma(t)$ can be calculated as follows:

$$\sigma(t) = \frac{5.1}{\sqrt{50 \times 100}} \times 10^{-6} \frac{\Delta k}{k} = 7.21 \times 10^{-8} \frac{\Delta k}{k} = 0.00096\ cents \quad [2]$$

Other design constraints that should be considered before installing an open loop in NRAD are the lack of available space and limited excess reactivity (50 cents). Proper material selection for the tube, location of oscillator tube insertion and detection method were studied for the design which can be found in the later chapters.

Chapter 2: LITERATURE REVIEW

2.1. Avery Theory of Coupled Reactors

After the Second World War, the theory of coupled-core reactors began to be developed and was reviewed by R. Avery at the Argonne National Laboratory (Ash, 1965). His theory of the coupled reactors implies that two assemblies (e.g. a thermal and a fast core) are physically coupled in the way that some neutrons originated in a region might have been generated in some other regions (Ash, 1965). Kinetics behavior of such reactors would be different than those in the un-coupled reactors. ATR-C (Advanced Test Reactor -Critical) with four different lobes could be thought of four different reactors coupled together in a complex manner.

2.2. Eigenvalue Separation (EVS) Technique

EVS technique was studied by Om Pal Singh and Obaidurrahman K in a paper titled"Investigation on Neutronic Decoupling Phenomenon in Large Nuclear Reactors" (Singh, 2010). They used the characteristic size of the nuclear reactors as a fundamental basis to assess the degree of coupling/ decoupling. Later, they used EVS to optimize the core geometry of a pressurized water reactor with minimum influence of the higher harmonics.

2.3. Pile Oscillator

The detailed theory behind the pile oscillator can be found in any textbook on reactor kinetics. It was used to measure the reactivity fluctuations. E.P. Wigner proposed

the theory of using periodic perturbations on reactivity to modulate the neutron population during the Manhattan Project days. It was thought of as an effective way of measuring absorption cross-sections. In this method, an absorber was introduced into a critical reactor. This will cause an alteration in the neutron population and make the reactor sub-critical. Then the reactor was brought to critical by using a calibrated control rod. From the amount of reactivity that was required to insert to bring the reactor back to critical, the absorption cross-section of the sample inserted could be ascertained. This was later extended to measure the reactivity insertions.

2.4. A Pile Oscillator for AGN 201 Reactor

James R. Roney in 1959 wrote a thesis on implementing a pile oscillator for AGN 201. He chose the already installed ion chamber and a linear amplifier on the control console to provide data from the pile oscillator. During that time reactor noise was not extensively studied and it was believed that some errors on measurement were caused due to the noise (Roney, 1959).

2.5. Reactor Kinetics, Transfer Function

Theories presented in the textbook “Dynamics of Nuclear Reactors” by David L. Hetrick were extensively used in preparing this thesis (Hetrick, 1993). These concepts include the derivation of the point reactor kinetic model from neutron diffusion and transport theory, solution of the point kinetic model along with the characteristic roots of the in-hour equation, derivation of the inverse kinetic equation to get reactivity equation from given power history and study of the transfer function.

2.6. ATR-C and NRAD References

The paper "Advanced Test Reactor: Serpentine Arrangement of Highly Enriched Water-Moderated Uranium-Aluminide Fuel Plates Reflected by Beryllium" evaluated by Soon S. Kim, Bruce G. Schnitzler at Idaho National Laboratory, provided the detailed description of ATR (Kim, 2005). Moreover, the same input listing provided in the appendix of this paper was used to obtain the flux profile across the core.

The paper entitled "Fresh-Core Reload of the Neutron Radiography (NRAD) Reactor with Uranium-Erbium-Zirconium-Hydride Fuel" by John Bess et al. gave the detailed description of the NRAD reactor (Bess, 2010).

2.7. Other Related Resources

In preparing this thesis, several papers were studied. The most relevant ones are: "The Calibration of the Follower Rod for the ISU-AGN-201 Reactor" by Tony Riley (Riley, 2013), "Comparisons of Open Loop and Closed Loop Reactivity Measurement Technique on the ISU-AGN-201 Reactor" by Ben Baker (Baker, 2013), and "Development and Testing of an Open-Loop Oscillator for Small Reactivity Worth Samples", a proposal to the U.S. Department of Energy by Prof. George Imel (Imel, 2010). The main objective of all these documents was to demonstrate the possibility of an open- loop technique to measure small reactivities with similar or better accuracy and precision than that with the closed- loop. If that is the case, open loop devices could be implemented in other facilities.

Chapter 3: THEORY

3.1. Neutron Basics

Since the discovery of nuclear reactors, neutrons have been important particles of interest. A neutron is a neutral particle with mass slightly greater than that of a proton. It is not stable except when bound into the nucleus with the nuclear force. This force is the only significant force that needs to be taken into account during diffusion of neutrons.

In a nuclear reactor, the number of neutrons present at any instant of time is negligible as compared with the number of atomic nuclei present in that infinitesimal volume so, the mutual collisions of the neutrons may be neglected without any loss of generality. Furthermore, neutrons have no interactions with the electron cloud due to its uncharged nature, so neutrons only collide with the nuclei. Neutrons may interact with nuclei in a number of ways such as elastic scattering, inelastic scattering, radiative capture, charged-particle reactions, neutron-producing reactions and fission.

Fission is the type of interaction in which a neutron is absorbed into a heavy nuclide (e.g. U-235) which then splits into its constituent particles with a release of energy. As an example of such a reaction, consider a neutron incident on a Uranium-235 nucleus: (Duderstadt, 1976)

$$Neutron + U - 235 \rightarrow Fisson\ products + More\ neutrons + Energy \qquad [3]$$

The probability that the neutrons interact with the nuclei is given by the cross-section. Mathematically,

$$\sigma = \frac{\frac{\text{Reactions}}{\text{nucleus}}/\text{sec}}{\frac{\text{neutrons}}{\text{cm}^2}/\text{sec}} \quad [4]$$

Where, σ is the microscopic cross-section.

In a reactor the number of neutrons may decrease (sub-critical), increase (super-critical) or be constant (critical) from one generation to another generation.

Mathematically,

$$Multiplication\ \ factor\ (k) = \frac{Number\ of\ neutrons\ in\ one\ generation}{Number\ of\ neutrons\ in\ preceeding\ generation} \quad [5]$$

The value of k is a measure of behavior of the chain reaction in reactor control. The reactor is sub-critical when k<1, critical when k=1, and super-critical when k>1. When k=1, the number of neutrons in any two consecutive generations are equal and the chain reaction will be independent of time. Thus, k can be thought as an eigenvalue associated to some flux as an eigenfunction.

3.2. Eigenvalue

An eigenfunction expansion method has been used to solve the boundary value problems as an expansion in a set of normal modes called eigenfunctions. An eignevalue problem has the following form:

$$H\psi_n = \lambda_n \psi_n \quad [6]$$

Where, ψ_n is the eigenfunction corresponding to the eigenvalue λ_n with H being an operator (transport operator in our case)

3.2.1. Eigenvalue in ATR-C

ATR-C has a complex geometry that has neutronic coupling between the core zones, and there is the possibility of having larger sensitivity to the flux distribution due to the local perturbation. Realizing the complexity in geometry, we decided to use the eigenvalue separation (EVS) technique to study the influence of the higher harmonics on the stability by coupling/decoupling. In EVS, higher harmonics of the neutron flux derived from the diffusion equation are evaluated and their relative influence on the neutron flux tilt forms the basis of the neutron coupling. In order to get an idea behind the EVS, an illustration of a simple eigenvalue equation and buckling to get the eigenvalue separation in a spherical core is demonstrated below: (Singh, 2010)

$$\lambda_n = \frac{\mathrm{k}_\infty}{1 + \mathrm{M}^2 \mathrm{B}_\mathrm{n}^2} \quad [7]$$

Where λ_n is the nth harmonics, M^2 is the migration area, B_n^2 is the geometric buckling, k_∞ is the infinite multiplication factor.

Eigenvalue separation (ε) between the first mode and the fundamental mode is expressed as (Singh, 2010)

$$\varepsilon = \frac{1}{\lambda_1} - \frac{1}{\lambda_0} \quad [8]$$

Using the above two equations, EVS was found to be approximately

$$\varepsilon = 3\frac{M\pi^2}{R} \quad [9]$$

Where, R is the extrapolated radius of the core.

Equation 9 shows that EVS is inversely proportional to the size of the core. The smaller the core is the larger is the EVS. Larger EVS suggests that the effect of higher harmonics to the flux decreases more rapidly and more quickly the fundamental mode is attained. This was for a defined spherical core but ATR-C has a complex system and is lot more difficult. So, several modes are needed to clearly describe the flux in ATR-C.

3.2.2. Higher Modes and Expansion Coefficients

The flux profile that describes the ATR-C reactor was determined first by using the MCNP code (Kim, 2005). A function that fits the flux profile is then determined in order to calculate the expansion coefficients of the higher harmonics. These harmonics could later be used as an estimation of the neutronic coupling/decoupling phenomenon through the eigenvalue separation (EVS) technique. To get a function that fits the flux profile precisely was difficult due to the complications in the geometry. Nevertheless, numerical integration could be used to get an estimate and a mathematical fit of the complex power also gave a close match.

An arbitrary function that fits the flux can then be expanded in spherical harmonics as (Jackson, 2007)

$$g(\theta,\phi) = \sum_{m=l}^{-l} A_{lm} Y_{lm}(\theta,\phi) \qquad [10]$$

With the coefficients given by,

$$A_{lm} = \int d\Omega\, Y_{lm}(\theta,\phi) A_{lm}(\theta,\phi) \qquad [11]$$

As mentioned before, the flux profile could also be approximately fitted with some function of a complex power. This function could be expanded in spherical harmonics to get the higher modes. In order to get the accurate results, the choice of coordinate system is vital.

The flux profile obtained from the MCNP simulation is in the rectangular coordinate system (LANL, 1957). This system is transformed to the spherical coordinate system so that the spherical harmonics expansions could be used to find the coefficients. These coefficients could then be analyzed to see the coupling from the higher harmonics. Transformations are given as follows.

$$Cartesisn \leftrightarrow Spherical \qquad [12]$$
$$x = r\,Cos\theta\,Sin\phi, y = r\,Sin\theta\,Cos\phi, z = r\,Cos\phi$$
$$r = \sqrt{x^2 + y^2 + z^2}, \theta = arc\,Tan\frac{y}{x}, \phi = arc\,Tan\frac{\sqrt{x^2+y^2}}{z}$$

Where, r is the radius in meters, θ is the polar angle in radians and ϕ is the azimuthal angle in radians

3.3. Reactor Kinetics

The time behavior of the neutron population in any reactor caused by the alteration in the multiplication factor is studied in reactor kinetics. The degree of the change in the neutron population can be estimated by measuring the reactivity.

The basic definition of the reactivity is given by the equation 13 below:

$$\rho = \frac{k-1}{k} \qquad [13]$$

$$\rho[Dollars] = \frac{k-1}{k\beta_{eff}}$$

Where, ρ is the reactivity, k is the multiplication factor given by the equation 5. Reactivity in dollars can be obtained by dividing $\Delta k/k$ by the delayed neutron fraction β_{eff} as shown in equation 14. A reactivity of one dollar is the same as reactivity equal to effective delayed neutron fraction (β_{eff}) and a reactivity of one cent is equal to one-hundredth of a dollar. $\Delta k/k$ is normally expressed as a percentage, or in dollars by dividing by the effective delayed neutron fraction, or pcm (percent milli). The in-hour is rarely used nowadays to express reactivity. We will use dollars and cents in this thesis.

The point reactor kinetic equation describes the time-dependence of the neutron population in any reactor along with the effect of the delayed neutron precursors. Several assumptions are made to get a simplified equation and can be generalized later. The most significant ones are: the one-speed diffusion theory approximations (neutrons are characterized by a single speed, uniform medium with constant cross-section, isotropic scattering in the lab system), flux is separable in time and space, equation of continuity is valid, etc.).

The equation of continuity is a mathematical expression that describes the balance of neutrons in a specified volume (reactor) (Lamarsh, 2001).

$$\begin{aligned} Rate\ of\ change\ in\ neutrons\ in\ volume \\ = [Rate\ of\ production\ of\ neutrons\ in\ volume] \\ - [Rate\ of\ absorption\ of\ neutrons\ in\ volume] \\ - [Rate\ of\ leakage\ of\ neutrons\ from\ volume] \end{aligned} \quad [14]$$

This can be expressed mathematically by the neutron diffusion equations:

$$\frac{1}{v}\frac{\partial \phi}{\partial \mathrm{t}} - \mathrm{D}\nabla^2\phi + \Sigma_a\phi(r,t) = (1-\beta)v\Sigma_f\phi(r,t) + \sum_{i=1}^{6}\lambda_i C_i\,(r,t) \quad [15]$$

$$\frac{\partial C_i}{\partial t} = \beta_i v\Sigma_f\phi(r,t) - \lambda_i C_i(r,t) \quad [16]$$

Where, v is the neutron speed in cm/s, ϕ is the neutron flux with the units of $\frac{\#\ of\ neutrons}{cm^2 second}$, t is the time in seconds, D is the diffusion constant with the units of cm, ∇^2 is the Laplacian operator, $\Sigma_a$is the macroscopic absorption cross-section of any material with the units of cm^{-1}, $\Sigma_f$is the macroscopic fission cross-section of any material with the units of cm^{-1}, $C_i(r,t)$ is the precursors concentration with the units of $\frac{\#\ of\ precursors}{cm^3}$, λ_i is the decay constant of the ith group with the units of sec^{-1}, β_i is the delayed neutron fraction (fraction of the delayed neutrons from group "i" to total number of neutrons). The presence of the delayed neutrons is crucial in reactor control and the kinetic behavior of the reactor. These delayed neutrons fit into six groups

Equations 15 and 16 are two differential equations describing the neutron flux in a reactor including the delayed neutron precursors. These equations can be solved by using the separation of variable technique i.e. both the flux and the precursor concentration can be written as separable functions of space and time.

$$\phi(r,t) = vn(t)\psi_1(r) \quad [17]$$

$$C_i(r,t) = C_i(t)\psi_1(r) \quad [18]$$

Where, $\psi_1(r)$ is the fundamental mode that describes the spatial flux profile. Precursors are assumed to have the same spatial flux distribution as the flux.

Solving equations 15 and 16 using the separation of variable i.e. equations 17 and 18 with few substitutions, we arrive at the point kinetic equations:

$$\frac{dn(t)}{dt} = \left[\frac{\rho(t)-\beta}{\Lambda}\right] n(t) + \sum_{i=1}^{6} \lambda_i C_i\,(r,t) \quad [19]$$

$$\frac{dC_i}{dt} = \frac{\beta}{\Lambda}\mathrm{n(t)} - \lambda_i C_i(r,t) \quad [20]$$

Where, Λ is the generation time [seconds]

The point reactor kinetic equations consist of set of seven coupled differential equations, the solution of which is difficult without approximations. Moreover, the equations can be non-linear as the reactivity can be a function of time and depend on the neutron populations itself. To simplify the problem, let us imagine a reactor operating steady state ($\rho = 0$) at some operating power P_0 prior to t=0, when suddenly a reactivity ρ_0 is inserted. Assume that the sum of all the delayed neutrons can be represented as β and an averaged decay constant (Duderstadt, 1976)

$$\lambda = \lambda_{avg} = \left[\frac{1}{\beta}\sum_{i=1}^{6}\frac{\beta_i}{\lambda_i}\right]^{-1} \quad [21]$$

After these simplifications, the point reactor kinetic equations 19 and 20 reduce to the one group representation:

$$\frac{dP}{dt} = \left[\frac{\rho_0 - \beta}{\Lambda}\right] P(t) + \lambda C(t) \quad [22]$$

$$\frac{dC}{dt} = \frac{\beta}{\Lambda} \mathrm{P(t)} - \lambda C(t) \quad [23]$$

For $t < 0$, we have the equilibrium conditions:

$$\frac{dP}{dt} = \frac{dC}{dt} = 0 \rightarrow C(0) = \frac{\beta}{\lambda\Lambda} P_0 \quad [24]$$

$$P(0) = P_0 \quad [25]$$

Equations 22 and 23 are now the differential equations with the specified initial values and can be solved by several techniques like assuming the exponential solutions, laplace transform etc. A simple exponential method is used in this thesis.

Assume:

$$P(t) = Pe^{st} \quad [26]$$

$$C(t) = Ce^{st} \quad [27]$$

Where, P and C are some constants that are determined by using initial values.

Substituting these equations 26 and 27 in equations 22 and 23 we get a set of algebraic equations that will give a characteristic equation with two roots:

$$\Lambda s^2 + (\Lambda\lambda + \beta - \rho_0)s - \rho_0\lambda = 0 \quad [28]$$

Equation 28 is a quadratic equation that has two roots, and hence general solutions can be written in the form (Duderstadt, 1976)

$$P(t) = P_1 \exp(s_1 t) + P_2 \exp(s_2 t) \quad [29]$$

$$C(t) = C_1 \exp(s_1 t) + C_2 \exp(s_2 t) \quad [30]$$

The constants are determined by using the initial conditions and the roots are approximately found to be:

$$s_1 \cong \frac{\lambda \rho_0}{\beta - \rho_0} \quad [31]$$

$$s_2 \cong -(\frac{\beta - \rho_0}{\Lambda}) \quad [32]$$

The reactor period is simply the reciprocal of s_1

The characteristic equation 28 may be rearranged to get the in-hour equation, i.e.

$$\rho_0 = \frac{s\Lambda}{s\Lambda + 1} + \frac{1}{s\Lambda + 1} \frac{s\beta}{(s + \lambda_i)} \quad [33]$$

This equation 33 gives the decay constants for any constant reactivity insertion. In general, for six delayed groups, this equation would be modified as below:

$$\rho_0 = \frac{s\Lambda}{s\Lambda + 1} + \frac{1}{s\Lambda + 1} \sum_{i=1}^{6} \frac{s\beta_i}{(s + \lambda_i)} \quad [34]$$

This is the in-hour equation that gives the decay constants as the roots of the seventh order polynomial. Graphical representation of the roots is depicted below:

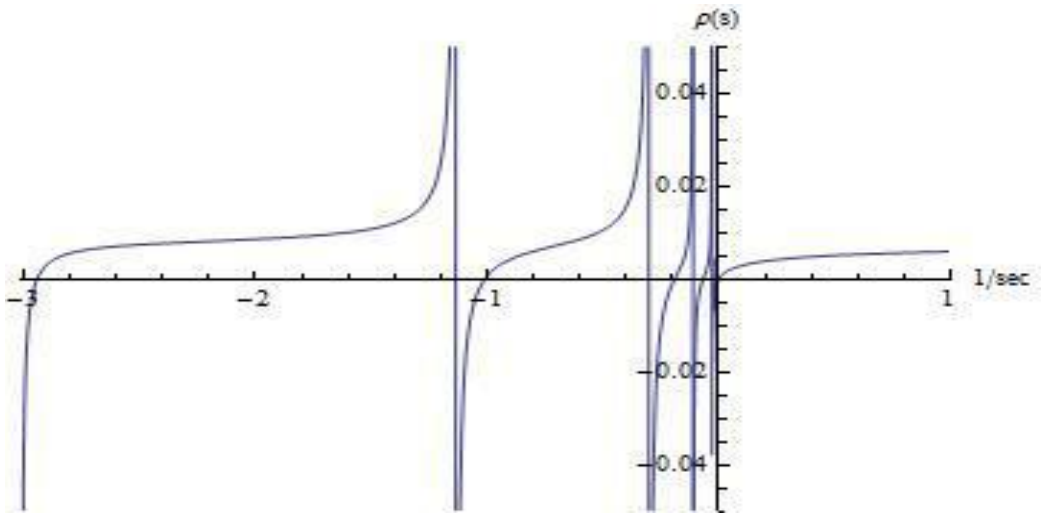

Figure 1. Roots of the In Hour Equation [Riley, 2011]

It can be seen from the graph that only one root is positive and the rest are negative. The reciprocal of the positive root is defined as the reactor period and the remaining roots are the transients that die out rapidly after a reactivity insertion.

The in-hour equation enables us to calculate the reactor period for a given reactivity change. As for instance, for the small reactivity insertions ($\rho_0 \ll \beta$), we are more interested in small reactivities measurements in this thesis), the in-hour equation reduces to (Duderstadt, 1976).

[35]

$$\rho_0 \cong s_1\Lambda + s_1 \sum_{i=1}^{6} \frac{\beta_i}{(\lambda_i)}$$

3.4. Reactor Transfer Function

The output (power) of any physical system (reactor) to a signal input (reactivity) applied to it can be studied with the help of the transfer function $H(s)$,

Mathematically,

$$H(s) = \frac{Laplace\ transform\ of\ the\ response\ (output)}{Laplace\ transform\ of\ input} \quad [36]$$

The block diagram with time and frequency domain can be found in figure 2 below:

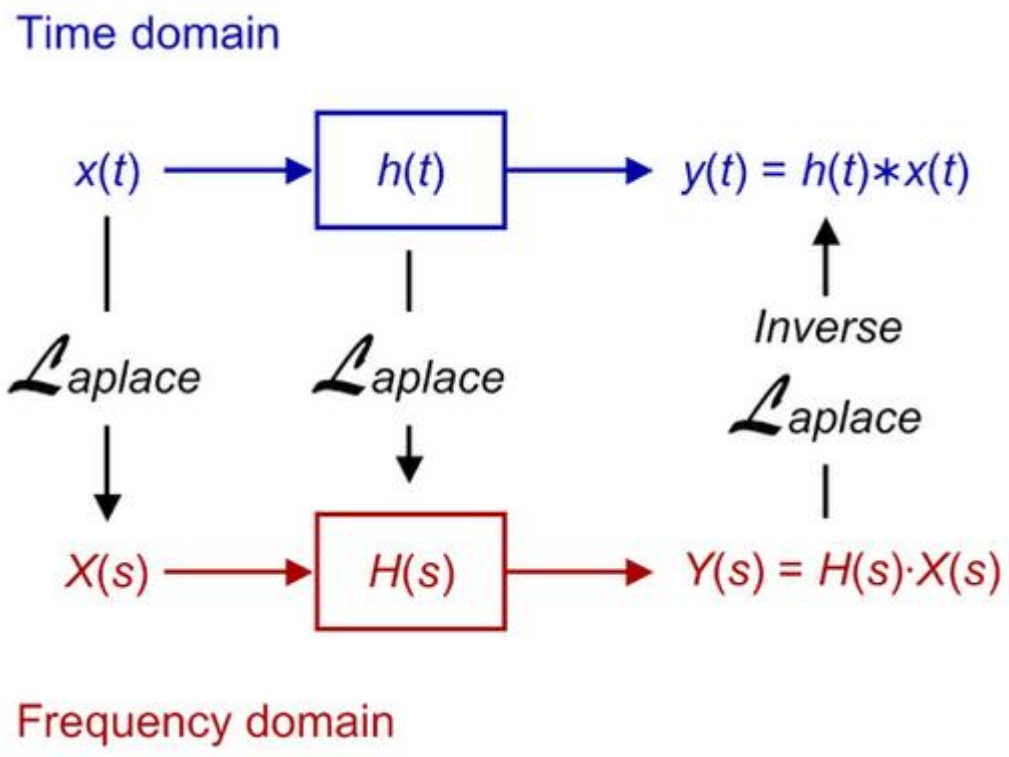

Figure 2. Transfer Function in Two Domains (en.wikibooks.org)

Depending on whether the output affects the input or not, the transfer function can be divided into open loop transfer function and closed loop transfer function. The following section explains those methods of determining transfer function in detail.

3.4.1. Closed Loop Technique

The technique in which the output (power) affects the input (reactivity) due to the feedback generated is known as the closed loop technique. In other words, a closed loop has a non-zero feedback. Feedback may be a positive or a negative depending on how it modifies the driving function of the system. If a response enhances the driving function, it is a positive feedback while if it inhibits the driving function, it is a negative feedback (Engen, 1970).

Figure 3 below presents the block diagram for the closed loop technique.

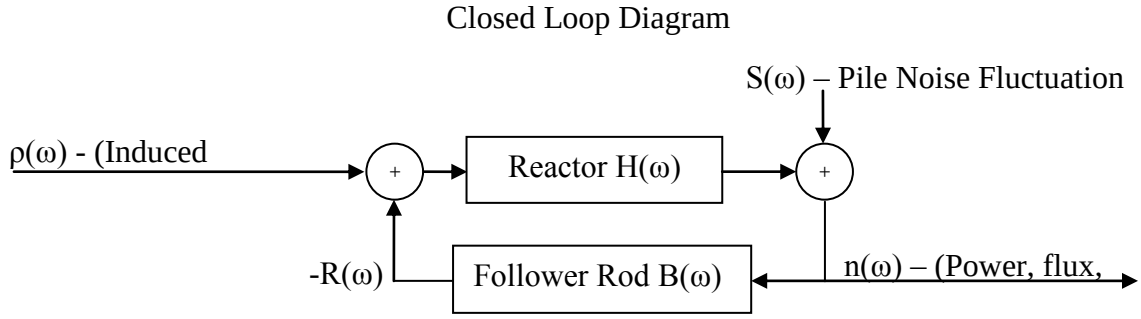

Figure 3. A Closed Loop Technique (Baker, 2013)

In a closed loop, an extra calibrated control rod is required to control the power, sometimes called the "pilot rod" (Riley, 2011). This technique has been in practice in the MINERVE reactor in France (Riley, 2011). Building and installing a second feedback control rod adds costs and complications, which is the driving force to validate the open loop technique. If it can be demonstrated that the open loop method is as accurate and

precise as the closed loop, then installation of it could be done in other reactors as done by Ben Baker in the simple AGN201 (Baker, 2013).

3.4.2. Open Loop Technique

The technique in which the output (power) does not affect the input (reactivity) is known as an open loop technique. In other words, an open loop has a no feedback influence. Figure 4 below depicts the block diagram of this method.

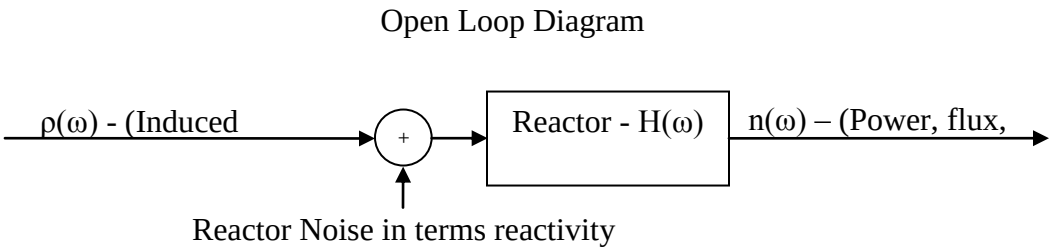

Figure 4. Open Loop Block Diagram (Baker, 2013)

An open loop technique can be called the pile oscillator method. E.P. Wigner, during the Manhattan Project days proposed the idea of using the periodic reactivity fluctuations to modulate the neutron density (Ash, 1965). In this method, a sample is introduced into a reactor core. Depending on whether a sample is an absorber such as boron or cadmium or a fission material, the total neutron population is altered. For instance, if a sample is an absorbing material and it is introduced into a critical reactor, some extra reactivity is needed to restore the reactor to critical. The absorption cross section of the material could then be ascertained as well as the reactivity worth of that sample oscillated.

It is to be noted that the open-loop transfer function of a reactor is valid for very low-power operation, often referred to as zero-power. At this power level, only the nuclear characteristics of the core will determine the magnitude of the transfer function as there is little temperature feedback (Ash, 1965). Measurement of the transfer function will determine the stability of the reactor. The open loop transfer function of any reactor can be computed from the fundamental nuclear parameters. A complete derivation of the reactivity transfer function for small oscillations (perturbation) is as follows:

3.4.3. Derivation of the Zero-Power Transfer Function

Before beginning, a few assumptions were made. Initially, the reactor is assumed to be in steady state where all the time derivatives are zero. We assume the point kinetic model is valid for small fluctuations about the equilibrium power, and we assume a small oscillation in reactivity, power, etc. about the equilibrium value. For such oscillations, average values can be assumed to be same as the equilibrium values which is not always true in case of the large amplitude oscillations (Hetrick, 1993). Moreover, for such small oscillations all the higher order perturbations could be easily ignored (linearization).

We perturb as follows:

[37]

$$N = N_0 + \delta N$$
$$C_i = C_{i0} + \delta C_i$$
$$\rho = \rho_0 + \delta\rho$$
$$q = q_0$$

With the initial conditions,

$$C_{io} = \frac{\beta_i N_0}{\lambda_i \Lambda} \quad [38]$$

$$q_o = -\frac{\rho_i N_0}{\Lambda} \quad [39]$$

Inserting these conditions to the point kinetic model equation, and linearizing yields:

$$\frac{d(\delta N)}{dt} = \left[\frac{\rho_0 \delta\rho + \rho_0 \delta N - \beta \delta N}{\Lambda}\right] + \sum_{i=1}^{6} \lambda_i \, \delta C_i$$

$$\frac{d(\delta \mathrm{C})}{dt} = \frac{\beta_i}{\Lambda}(\delta N) - \lambda_i(\delta C_i) \quad [40]$$

Applying the laplace transform

$$\delta N(s) = \int_0^\infty \delta n(t) e^{-st} \, dt \quad [41]$$

to the above linearized equations, we obtain

$$\mathrm{s}\delta N(s) = \left[\frac{n_0 \delta R(s) + \rho_0 \delta N(s) - \beta \delta N(s)}{\Lambda}\right] + \sum_{i=1}^{6} \lambda_i \, \delta C_i(\mathrm{s}) \quad [42]$$

$$\mathrm{s}\delta C_i(s) = \frac{\beta_i}{\Lambda}\delta N(s) - \lambda_i \delta C_i(\mathrm{s}) \quad [43]$$

Collecting, we can write the transfer function:

$$G(s) = \frac{\delta N(s)}{\delta R(s)} = \frac{N_0}{\Lambda s + \beta - \rho_0 - \sum_{i=1}^{6} \frac{\lambda_i \beta_i}{(s + \lambda_i)}} \quad [44]$$

3.4.4. Inverse Kinetics

In order to determine the reactivity of the given sample at a specified power level, the open loop technique uses inverse kinetics. Inverse kinetics helps determine the time-dependence of the applied reactivity deduced from specific power variation. Moreover, the interpretation of the power responses provides information about the feedback mechanisms in the reactor (Duderstadt, 1976). The governing equation to calculate the reactivity is as follows (Hetrick, 1993).

$$\rho(t) = \frac{dn(t)}{dt}\frac{\Lambda}{n(t)} - \frac{1}{n(t)}\sum_{i=1}^{6}\beta_i\left[n_0 e^{-\lambda_i t} + \lambda_i \int_0^t e^{\lambda_i(t'-t)} n(t')dt'\right] + \beta \quad [45]$$

3.5. Reactor Description

Two different reactors were studied in preparing this thesis. The first one was the ATR-C with the complex geometry and the second one was the NRAD. This research not only gives the fundamental phenomena in all these reactors but also helps the reader to find the similarities and the differences. Brief descriptions of the reactors follow:

3.5.1. ATR-C

The Advanced Test Reactor (ATR) is a high flux test reactor designed to study the effects of radiation on the structural materials and fuel bundles. Several medical isotopes have also been produced there. It is a 250 MW thermal reactor located at the Reactor Technology Complex of the Idaho National Lab (INL) (Kim, 2005). The basic difference

between ATR and ATR-C is that ATR-C is a low power facility with the same core material and geometry as the 250 MW ATR.

Towards the beginning of the research, it was proposed to use ATR-C for measuring small reactivity with the open loop technique. Unfortunately, due to the complex geometry and strong coupling among the lobes, a simpler reactor was sought. ATR-C core has four lobes with 40 fuel elements arranged in a serpentine annulus with nine flux traps. Figure 5 below depicts an XY view of the ATR-C (Kim, 2005).

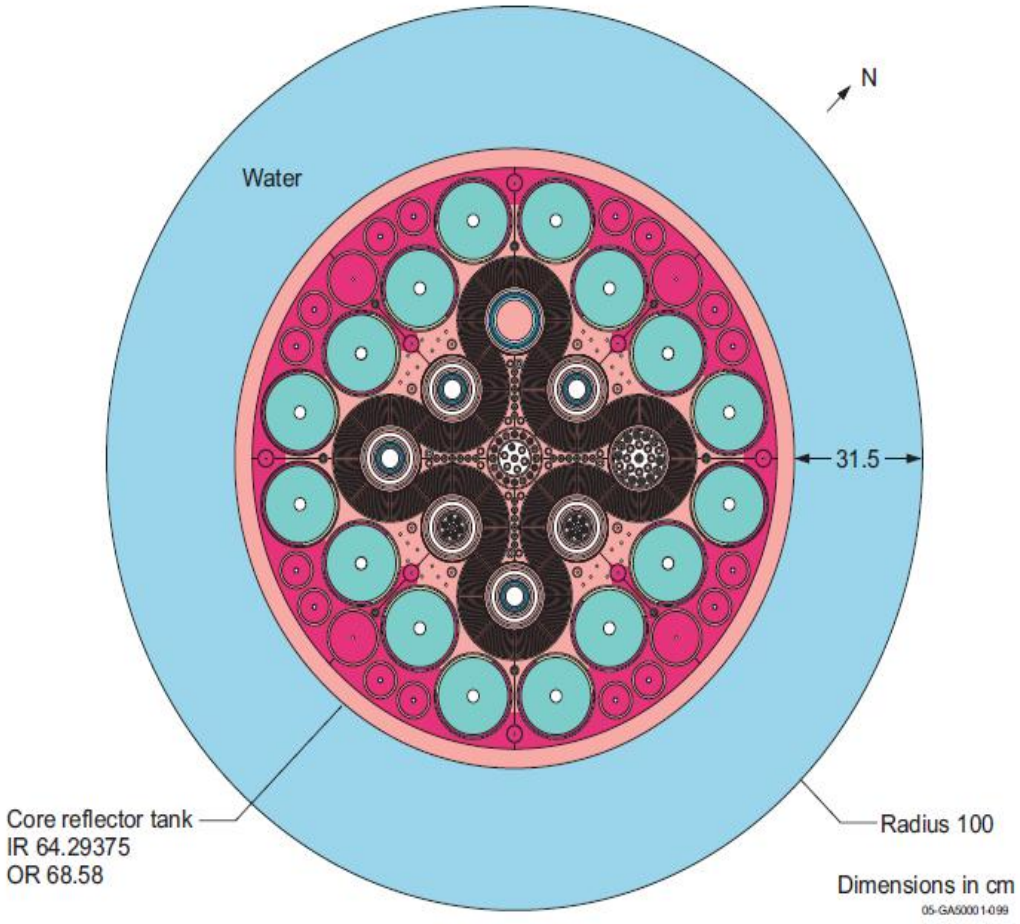

Figure 5. An XY View at x=0, y=0 of the Benchmark Model (Kim, 2005)

Each of the lobes presented above act as an individual reactor in that each lobe can operate at very different power levels. The flux profile obtained from one lobe might interfere with the other. This adds complication to get a fundamental mode.

3.5.2. AGN-201

The Aerojet General Nuclear -201 (AGN-201) reactor is located at the basement of the Lilibridge Engineering Building at Idaho State University. It is a low power reactor (licensed to 5W) primarily used for research and teaching purposes. It consists of uranium dioxide (UO2) as the fissile fuel homogeneously mixed with polyethylene. For the research purpose, the reactor has five experimental ports to allow the insertion of the materials in the core: four beam ports running north to south and a glory hole running east to west through the center of the core (Riley, 2011). Figure 6 below shows the broad view of the reactor.

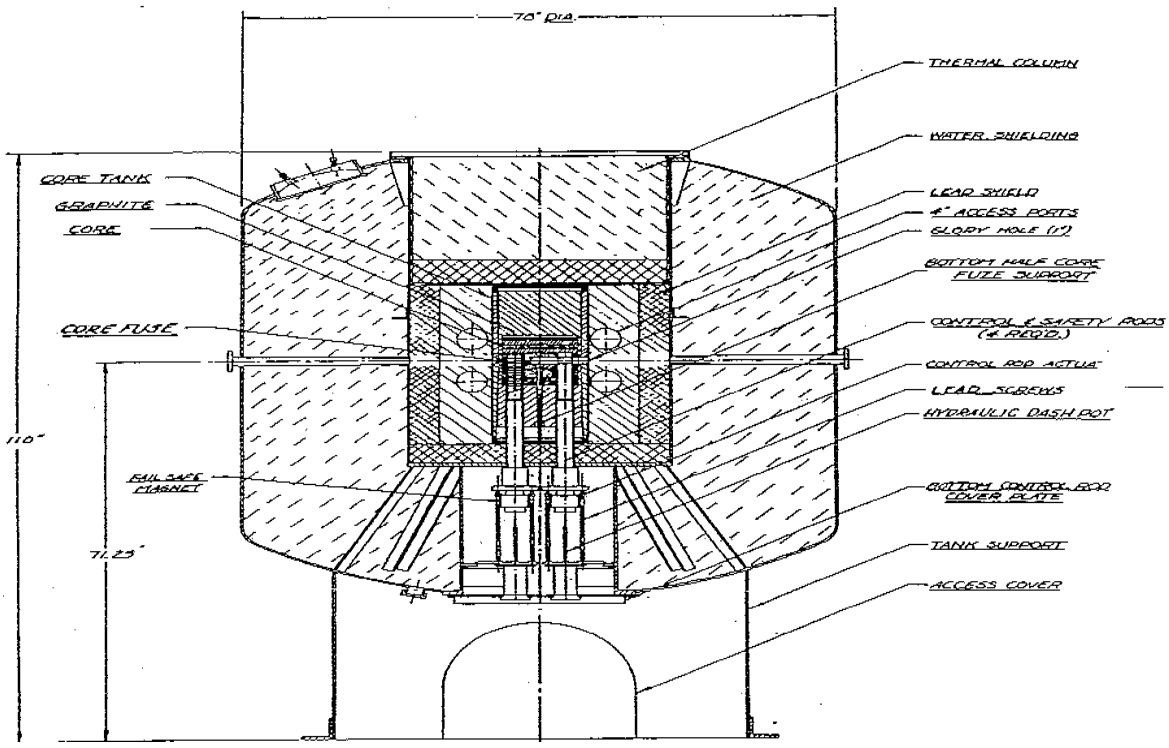

Figure 6. Broad View of the AGN-201 Reactor (Baker, 2013)

3.5.3. NRAD

The Neutron Radiography (NRAD) reactor is located in the basement of the Hot Fuels Examination Facility (HFEF) at the Materials and Fuels Complex at the Idaho National Laboratory (INL). It is a 250kW TRIGA reactor with a rectangular grid style core, which is used for conducting neutron radiography and performing specimen activation experiments. The reactor is inside a rectangular concrete confinement room located 120 feet from the control room. The reactor room is accessed by opening two shielded doors which seal off the room while the reactor is in operation. The reactor is covered by an additional shielded platform of which half is stationary and half slides on rollers to access the core (see figure 7). The reactor core is covered by water. The reactor

room is approximately 10 feet deep, 12 feet wide, and 17 feet in length, but it only has 5.5 feet of overhead clearance space for workers. This area also contains most of the pumping systems and additional electronic equipment that regulates the reactor as can be seen in Figure 7 below.

Figure 7. Reactor Design (John Bess)

Ben Baker had successfully calculated the effects of reactivity oscillations in the AGN-201 for his PhD dissertation (Baker, 2013). Due to the fact that NRAD has similar geometry and reactor parameters, we feel the same technique could be used to determine the reactivity of samples inserted with acceptable accuracy.

There are numerous design restraints that need to be considered before a system can be effectively and wisely chosen. One constraint that is imposed on this oscillator

design problem is that there is only a very small amount of excess reactivity available (50 cents). Thus, the solution cannot involve anything that will significantly lower the reactivity (e.g. air voids) and cause the reactor to become subcritical. Another constraint governing the scope of this problem is the amount of foundation space available near the core support assembly of the reactor core. The system must be able to fit in the space available.

Chapter 4: METHODOLOGY

4.1. ATR-C

The main purpose of this research was to use an open loop technique to estimate the reactivity worth of small samples in ATR-C. Neutron parameters such as neutron generation time, neutron lifetime, effective delayed neutron fraction, neutron flux profile across the core, etc. need to be estimated to get the transfer function of the reactor.

4.1.1. Procedure for ATR-C

For this thesis, MCNP input listings were provided from an NEA Benchmark (Kim, 2005). MCNP version 5 with continuous energy ENDF/B-V cross sections was used. The model used 1,250 active generations with 5,000 histories per generation. The first 50 generations were skipped. The evaluated continuous-energy ENDF/B-V cross-section data of the MCNP runs are based on 27°C (Kim, 2010). It is to be noted that MCNP input listings of ATR-C was used to build a model and this can be used in ATR-C. The flux profile, 3D plots and expansion coefficient calculations were done based on ATR-C data.

The flux profile and the corresponding 3D plot of the ATR-C were constructed. An approximate fit to the flux profile was performed to get a general function that describes the behavior. This arbitrary function was then expanded in spherical harmonics using the properties of orthogonally and completeness. Before expanding using spherical harmonics, the cartesian flux was transformed to the spherical coordinate system to have consistency in calculating the coefficients. More than ten expansion coefficients were

calculated using Mathematica 9.0.1 (Wolfram Research Inc., 2013). The input listing can be found in the Appendix. After finding the coefficients, they were used back in the expansion to see if the plots look similar to what they were supposed to be. All the coefficients build up to give the profile. A contour plot using the coefficients was also determined. Due to geometric coupling and complexity it was clear that ATR-C was not a good choice.

4.1.2. Results for ATR-C

Figure 8 below shows the calculated flux profile of the ATR-C. The clover leaf model with four different lobes corroborated the design. Conformal mapping was used to get the flux equation ($z^4=(x+iy)^4$, where the exponent is identified with the number of lobes of the clover leaf).

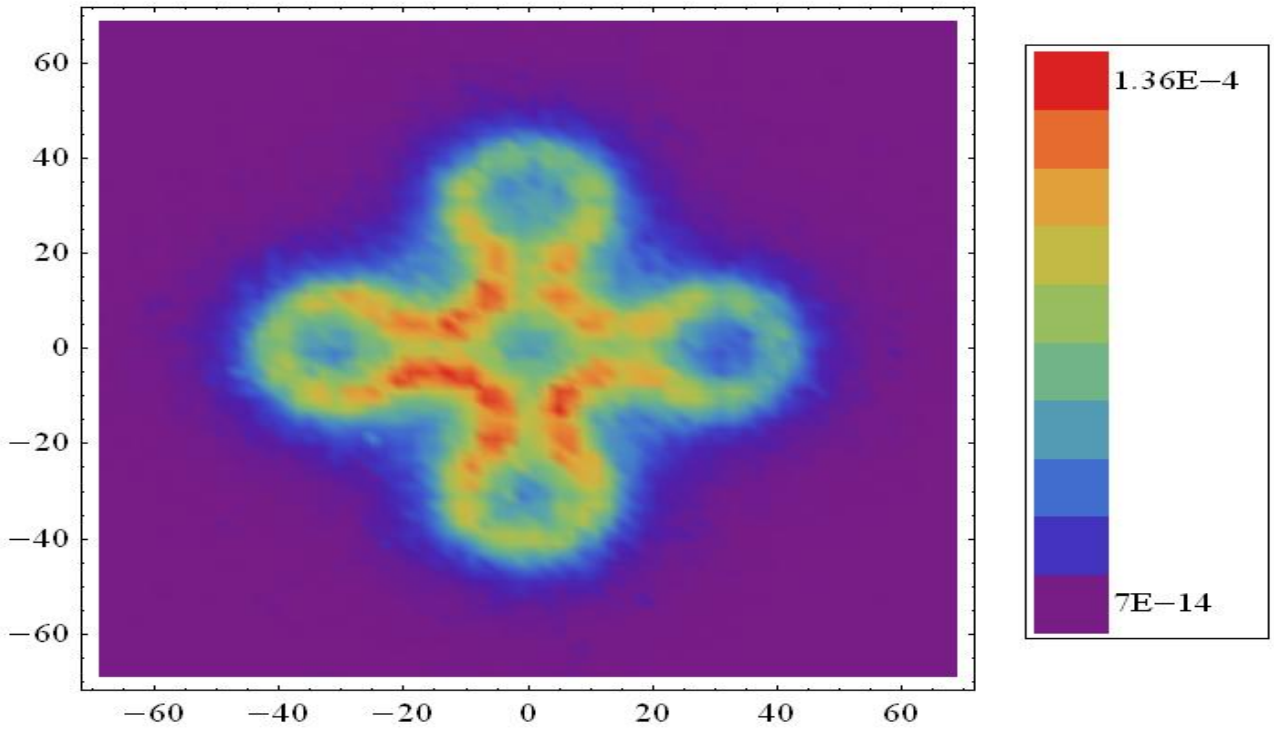

Figure 8. X-Y Flux Profile of the ATR-C Core

A similar plot 3D was constructed to better get the profile. Figure 9 below shows the plot.

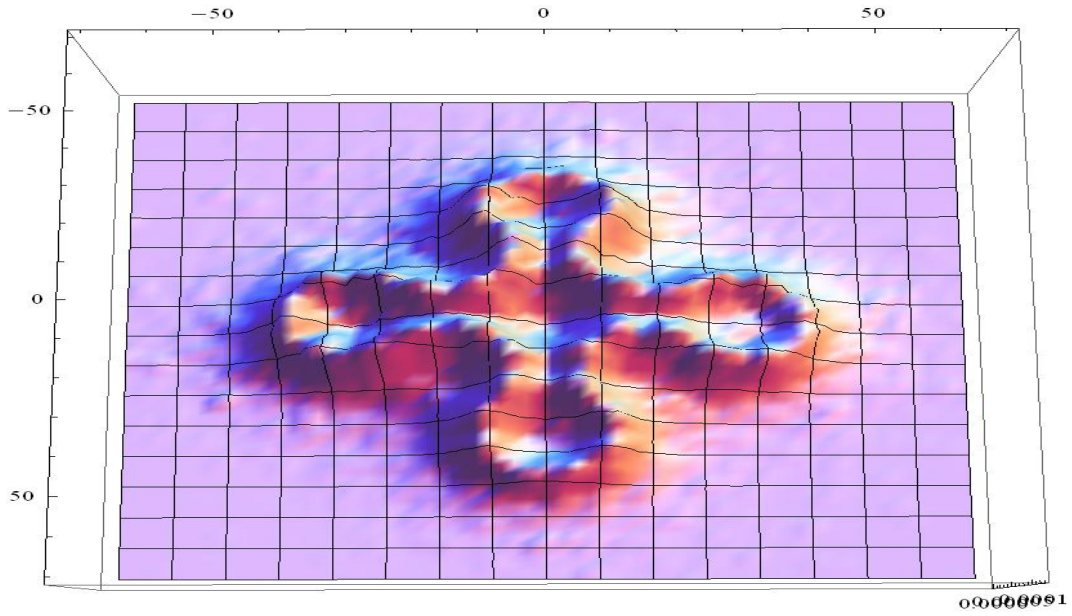

Figure 9. 3D Plot of the Flux vs X and Y across the ATR-C Core

Several expansion coefficients with varying “l” and “m” values are tabulated in the following table 1. There was not any specific pattern on how the coefficients which shows a large coupling among the lobes.

Table 1. Expansion Coefficients of ATR-C

S/N	Value of l	Value of m	Expansion Coefficient A_{lm}
1	0	0	5744.20
2	1	1	0
3	1	0	0
4	2	2	0
5	2	1	5528.50
6	2	0	3211.08
7	3	3	0
8	3	2	0
9	3	1	0
10	3	0	0
11	4	0	12696.90
12	5	0	0
13	6	0	9546.82
14	7	0	0
15	8	0	7740.09
16	9	0	0
17	10	0	6605.03
18	11	0	0

These coefficients clearly show that there is no rapidly converging fundamental mode in ATR-C. Thus, we could say that there is inadequate EVS to assume an uncoupled core. After obtaining the expansion coefficients, they were used to determine if they could reconstruct the profile. A similar contour plot was obtained with some approximations. Figure 10 below shows the corresponding contour plot.

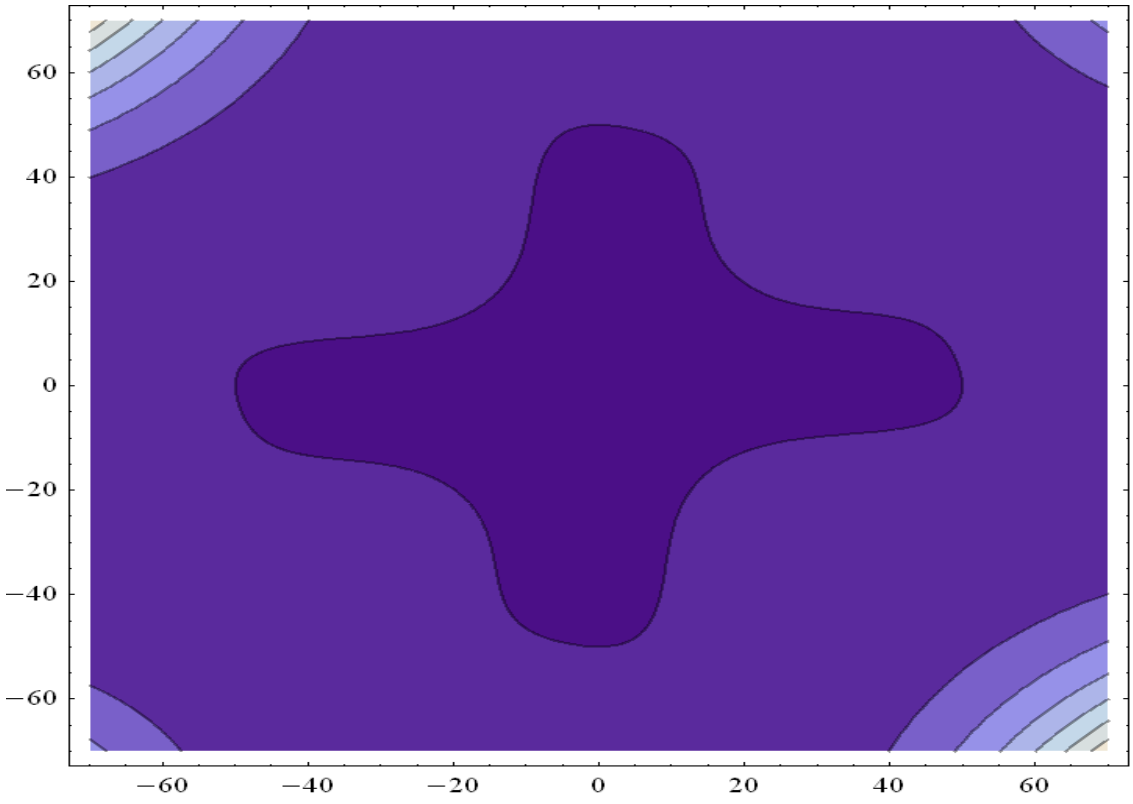

Figure 10. Contour Plot of ATR-C Core with the Expansion Coefficients

After realizing the complexity of ATR-C, it was decided to propose the open loop technique on a simpler reactor, i.e., NRAD**.**

4.2. NRAD

Similar work completed in the AGN-201 (Baker, 2013) gave an insight of the fact that an open loop technique could be used in NRAD, which has similar geometry and parameters. Before measuring the reactivity, kinetics parameters need to be ascertained. The parameters obtained are as follows (Bess, 2010).

Effective delayed neutron fraction (β_{eff}) = 0.0075

Neutron generation time = 24.5 microseconds

Decay constants of the precursor groups and the relative yields is given in the table below (Duderstadt, 1976).

Table 2. Delayed Neutron Yield and Half Life Data for U-235

Group	**$T_{1/2}$(sec)**	**Relative Yield**
1	54.51	0.038+/-0.004
2	21.84	0.213+/-0.007
3	6.00	0.188+/-0.024
4	2.23	0.407+/-0.010
5	0.496	0.128+/-0.012
6	0.179	0.026+/-0.004

The parameters were found to be of the same order of magnitude as those used in the ISU AGN-201. Using the NRAD parameters, a transfer function plot was obtained. This plot was then compared with that obtained using the AGN201 parameters. These plots can be found in the results section. KENO Va code was used to model the NRAD core. This code was validated before building the model (ORNL, 1998).

4.2.1. Validation of KENO Va for NRAD

KENO Va is the 3-dimensional Monte Carlo Code based computational method that can be used to determine the k-eff of a complicated system (ORNL, 1998). However, computed critical conditions must be validated for the reliability of the code. This code could then be used for the further modeling. In order to validate the code,

suitable benchmarks are selected. While selecting such benchmark experiments, the fuel enrichment, physical state, as well as the geometry and other components involved for storage must be considered.

The validation calculation involves the U9 benchmark assembly provided from NEA handbook (NEA, 2003). This benchmark was selected because of the cylindrical geometry of the core. Using the composition and their respective number densities provided in the handbook, k-eff was calculated to be 0.9901 ± 0.0016 from the SCALE/KENO 238-group calculation with ENDF/B-Model.

The KENO calculations were run with 203 generations with 1000 histories per generation, skipping the first three generations. The reported result of the k-eff in the handbook is 0.9954 ± 0.0024 (IEU-MET-FAST-010, page 58 of 102). Both the results are in good agreement with each other. The difference between the calculated k-eff and that obtained from the benchmark is called the bias. So, the bias was found to be 0.0053± 0.0008 which is less than 0.55%. The relative uncertainty in the ratio of C/R (calculated/reported) was found to be 0.994675507 by taking the square root of the sum of the squares of the calculated and benchmark uncertainties. The absolute uncertainty in the C/R ratio was found to be 0.002869083 by simply multiplying the C/R ratio with the relative uncertainty in C/R ratio. Table 3 below illustrates the results obtained for the validation. The input file can be found in the appendix.

Table 3. Validation and Uncertainty Results

		Benchmark			Absolute
Configuration	Calculated k-eff	Reported k-eff	C/R	Relative U (C/R)	Uncer in C/R
IEU-MET-FAST-010	0.9901+/-0.0016	0.9954+/-0.0024	0.994675507	0.002884441	0.002869083
			Close to 1	= SQRT (u1^2+u2^2)	= C/R * Relative U (C/R)

So, KENO Va could be used with accuracy and is valid.

4.2.2. Results for NRAD

Figure 11 below shows the plot of the transfer function comparing NRAD data with AGN-201 data. These plots were obtained by using MATLAB with the provided neutron parameters (The MathWorks Inc., 2010). Comparison of the transfer functions as seen on the plot below showed the feasibility and applicability of this technique to measure reactivity of small samples. NRAD was found to have a higher break frequency as compared to the AGN.

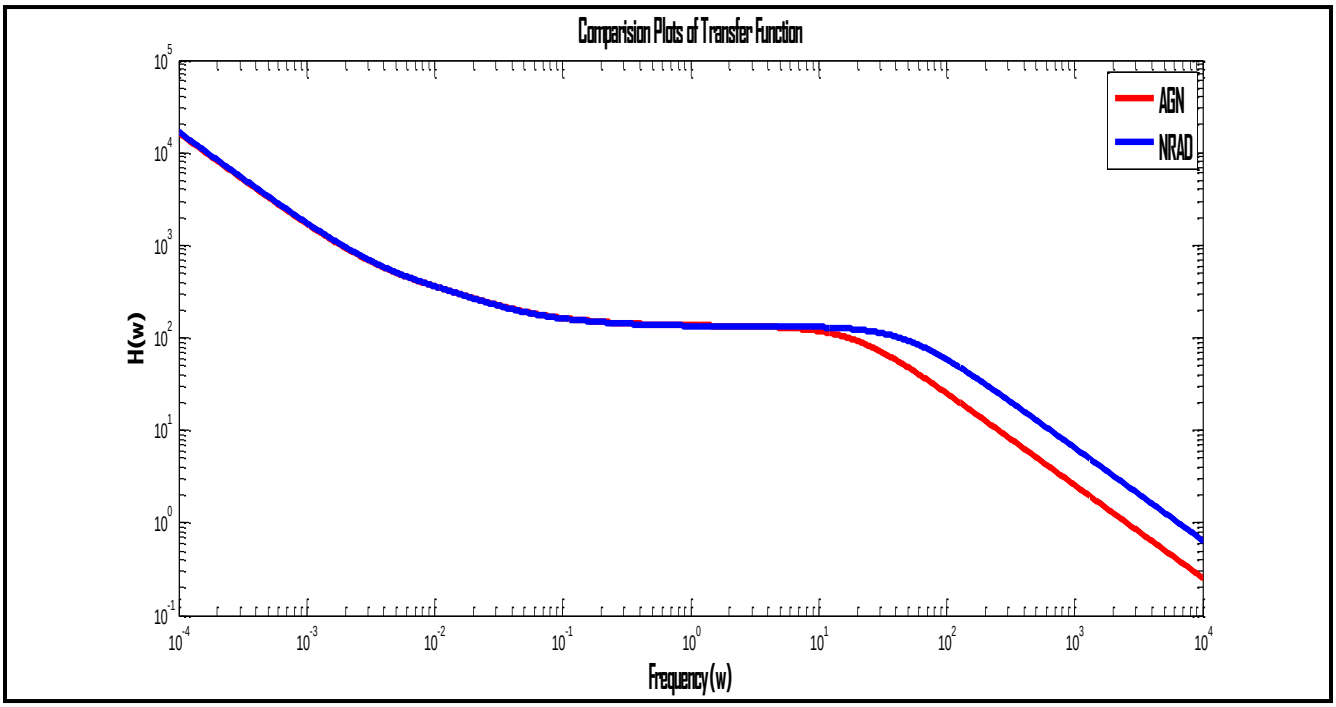

Figure 11. Comparison Plots of Transfer Function of AGN-201 and NRAD

Chapter 5. EXPERIMENT

After realizing the fact that open loop technique could be used in NRAD, a simple oscillator design is the next step towards the completion of the thesis.

5.1. Location of Oscillator

With the design constraints such as lack of excess reactivity (limited to 50 cents) and the lack of available space for an oscillator set up, an appropriate position need to be determined. The design should be such that the detectors are able to experience enough flux. The most suitable position for the reactivity perturbation is the center empty hole (irradiation position) which is shown in the figure 12 below.

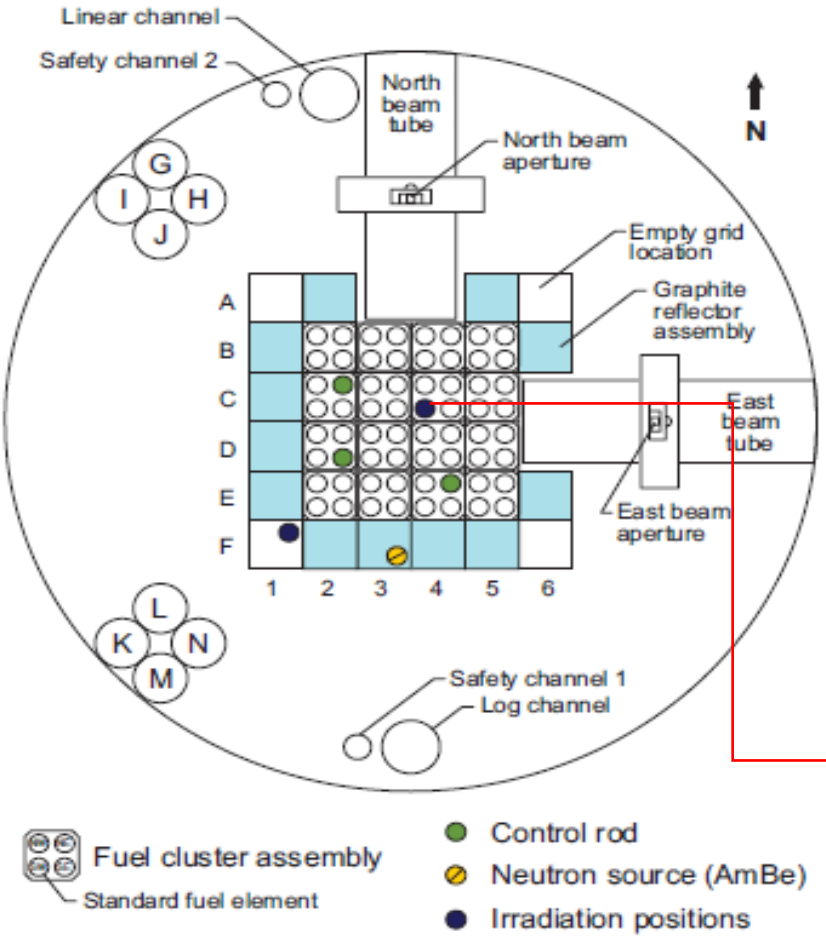

Figure 12. Best Location as an Irradiation position

5.2. Instrumentation

Table 4 below depicts several instruments that could be used in measuring reactivity. The purpose of each individual instrument with their model could also be found in the same table 4 .

Table 4. Instruments and Purpose

S/N	Type of Instrument	Purpose
1	Inonization Chamber (WL-8075 B-10)	To detect power/ flux/ neutron density
2	Linear Actuator	To drive the sample in a controlled fashion
3	Motor (Shinano Kenshi Brushless DC Motor)	To control the linear Actuator
4	Current Amplifier	To amplify the signals obtained form ionization chamber
5	Data Acquistion System (DAQ)	To sample obtained signal form the current amplifier
6	Pro-Motion Code	To set parameters in motor controller
7	Voltage Supply	To supply electrical energy to the motor and other instruments
8	LabView Program	To receive power information from DAQ and intrepret history
9	Cables	To provide necessary connections
10	Platform	To provide a stable and an appropriate assembly for the equipments

(LabVIEW National Instruments, 2013)

The equipment mentioned in the table 4 could be arranged as shown in figure 13 below to perform experiment.

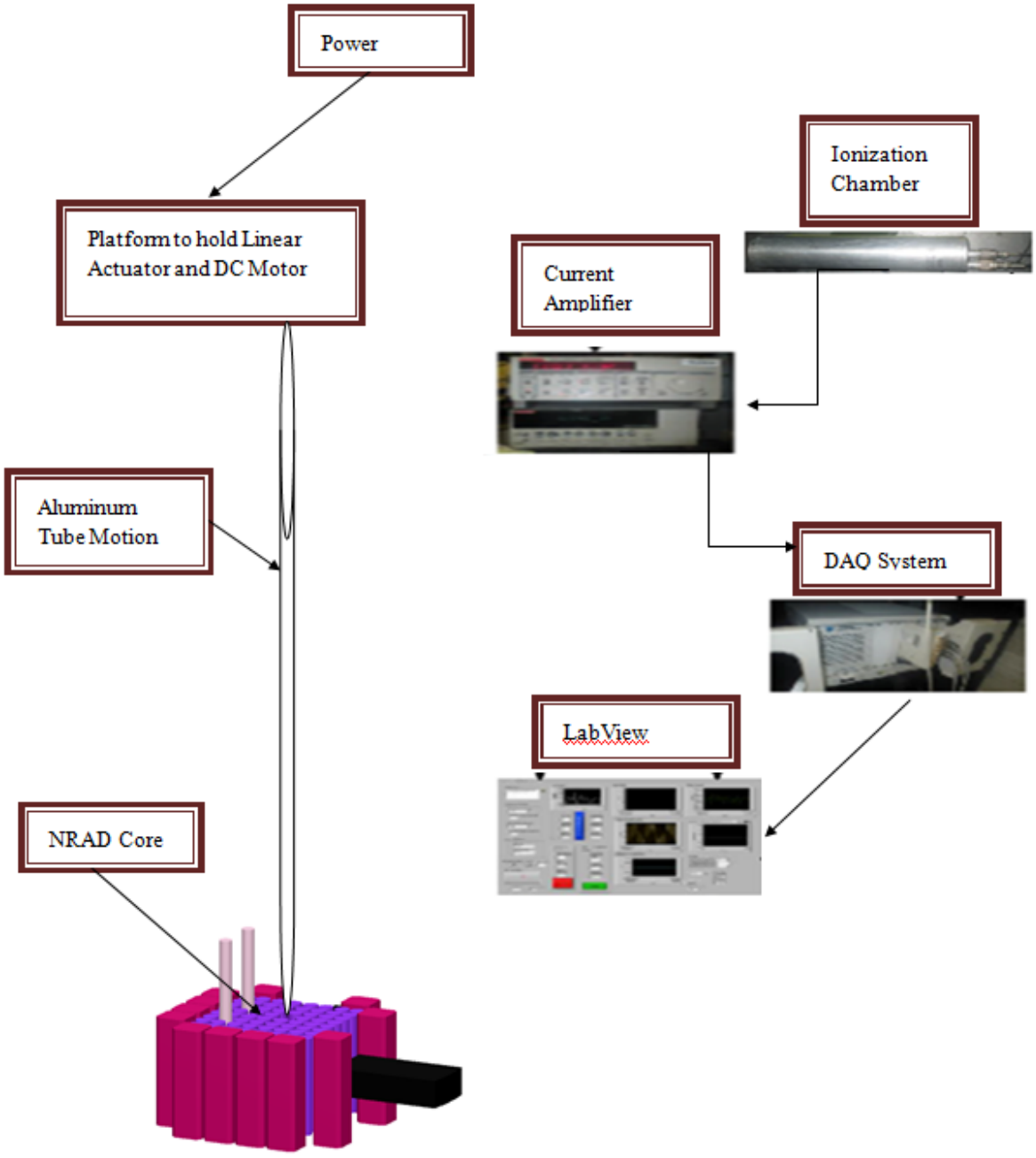

Figure 13. Experimental Set Up and Block Diagram for NRAD

5.3. KENO Model for NRAD

NRAD core was modeled with 60 fuel plate in KENO Va with 238 group ENDF/B-VII.0 neutron cross section data and other dimensions provided from NRAD Benchmark (Bess, 2010). Calculations of k-eff could also be performed to make sure the core is not super critical and safe to operate. Moreover, the estimates of k-eff will also help to determine the reactivity worth of the sample inserted. The KENO code was run with 1,550 generations with 100,000 neutrons per generation. The first 50 generations were skipped. This will result to 150,000,000 neutron histories. Figure 14 below shows a 3D model of NRAD core with oscillator location.

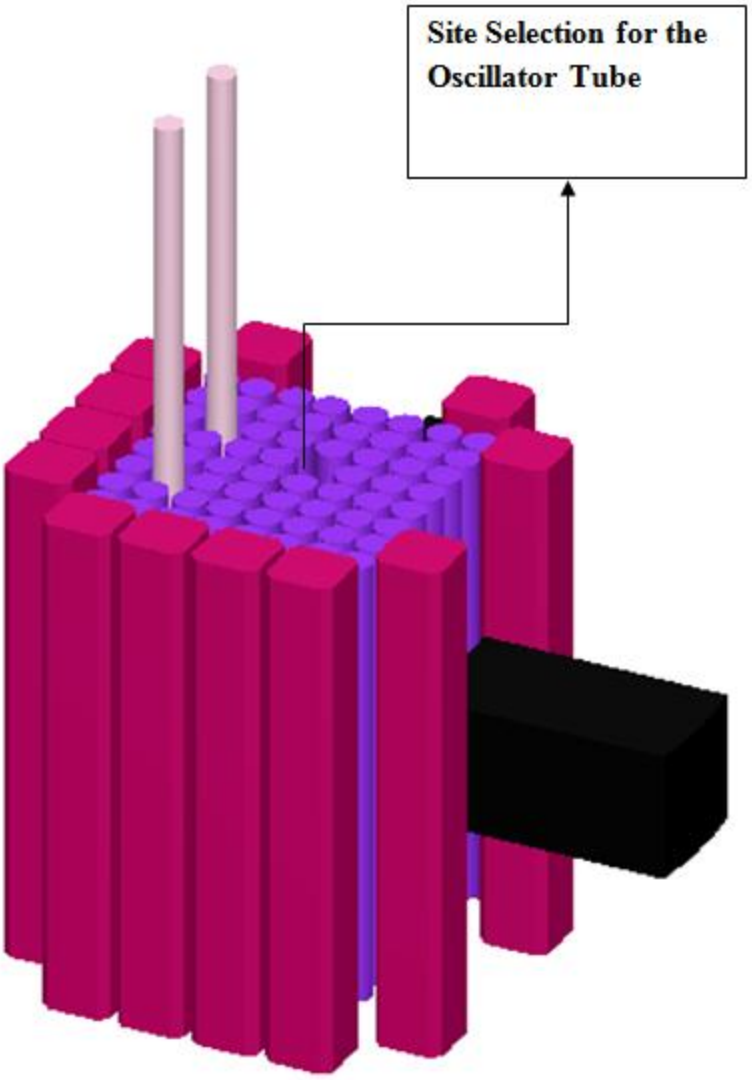

Figure 14. KENO 3D of NRAD with Aluminum tube location

Figure 15 below shows the top view of the NRAD core with positions of control rod and an oscillator rod. Figure 16 depicts the side view of NRAD.

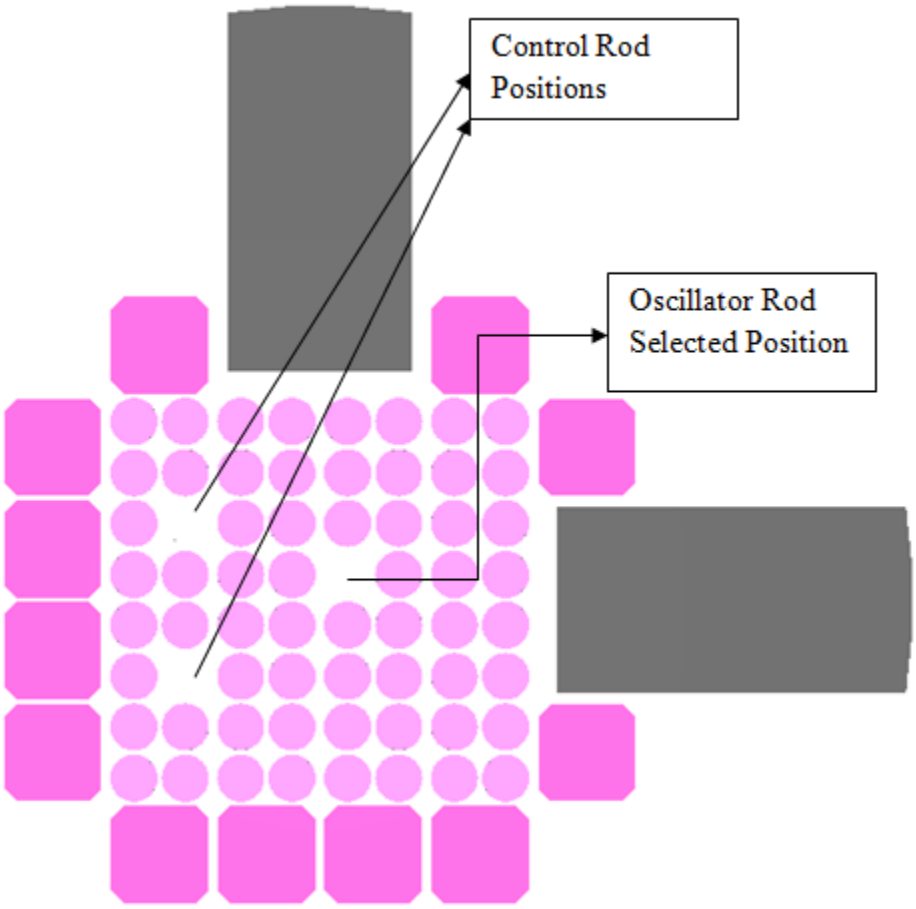

Figure 15. Top View of the NRAD Core

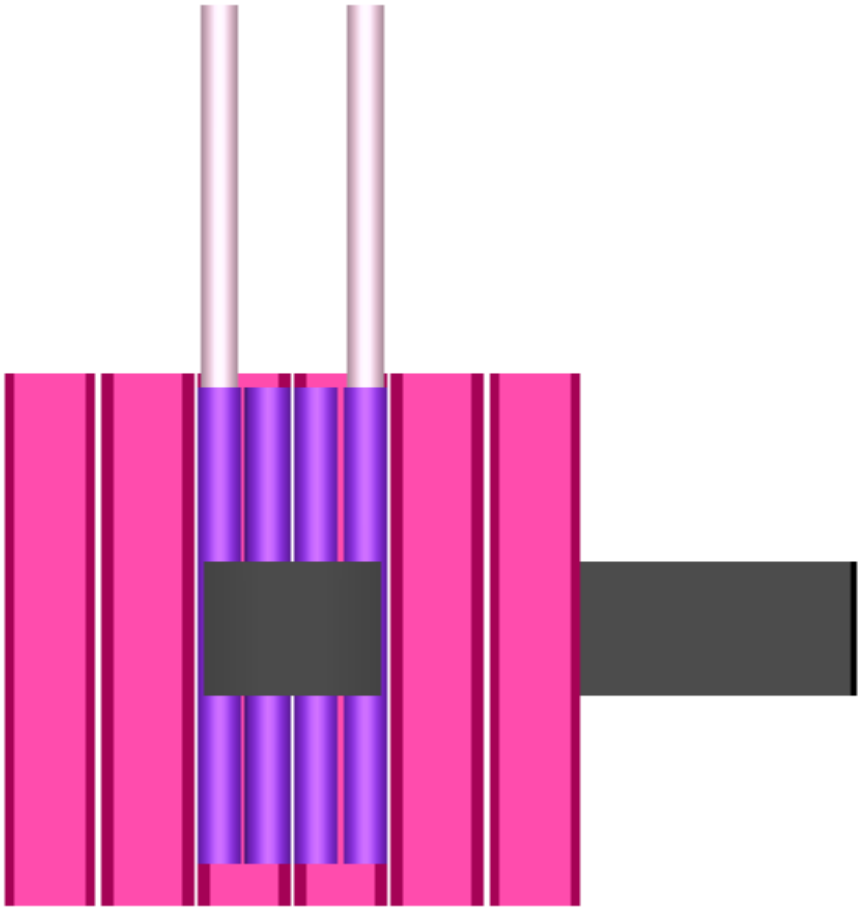

Figure 16. Side View of the NRAD Core

5.4. Conclusions for NRAD

KENO V.a can be used to model NRAD core with accuracy. This model can be used to see the effect of other simplifications that may occur such as replacing control rod guide tube with water, adding voids, or oscillating samples. This code can be used as a guideline to understand those components that cause maximum change in k_{eff}. Moreover, this code can be used for criticality safety with very little bias. The bias in the code may

be due to cross-section and/or code related. Reactivity worth of a sample oscillated can be obtained by comparing the k_{eff} with and without insertion.

The transfer function plots presented in the results section correlates the reactivity of the sample that caused perturbations. NRAD was found to have a higher break frequency than that of AGN-201. This was an expected result since break frequency is inversely proportional to neutron generation time ($f_{break} = \frac{\beta}{\Lambda}$). With this relation, break frequency was found to be around 306 Hertz. So, the reactor cannot respond beyond this frequency but passes the low frequencies. Similar behavior of NRAD and AGN-201 at low frequencies adds confidence in implementing the open loop technique to measure reactivity worth of small samples.

Chapter 6: CONCLUSIONS

A simple method of determining small reactivity using an open loop oscillator technique was successfully designed for the NRAD. This technique was initially proposed for Advanced Test Reactor at Idaho National Laboratory. Later, it was found that ATR-C was not a good choice due to its complex geometry (clover-leaf) and its characteristic of having a tremendous coupling of the higher harmonics with the fundamental mode. However, an open loop method was found to be a valid and a precise method to measure small reactivity in simpler reactors like Neutron Radiography (NRAD) and AGN-201.

Comparison of the transfer functions showed the feasibility and applicability of the open loop technique to measure reactivity of small samples. NRAD was found to have a spectrum with a higher break frequency as compared to the AGN-201.

Several plots such as: flux profile of the ATR-C core, 3 D plot of flux across ATR-C, plot with higher expansion coefficients of the ATR-C flux, transfer function plot of NRAD and its comparison with the ISU-AGN-201 reactor are also presented. After realizing the fact that this technique could be used in NRAD, a simple oscillator design is also presented in this thesis.

REFERENCES

1. Riley, Tony. *Calibration of Reactivity Oscillator for ISU-AGN-201 Reactor.* Pocatello : Idaho State University (Thesis), 2013.

2. Baker, Benjamin Allen. *Reactor Parameters for the ISU-AGN-201 Reactor.* Pocatello, Idaho : Idaho State University, 2011.

3. Baker, Benjamin Allen. *Comparisions of Open Loop and Closed Loop Reactivity Measurement Technique on the ISU-AGN-201 Reactor.* Pocatello, Idaho : Idaho State University, 2013

4. Imel ,George.*Development and Testing of an Open-Loop Oscillator for Small Resctivity Worth Samples.* Pocatello, Idaho : Idaho State University, 2013. Proposal.

5. James J. Duderstadt, Louis J. Hamilton. *Nuclear Reactor Analysis.* s.l. : John Wiley & Sons, inc., 1976.

6. Hetrick, David L. *Dynamics of Nuclear Reactors.* La Grange Park, Illinois : American Nuclear Society, 1993.

7. Nehari, Zeev.*Conformal Mapping.* New York:McGraw-Hill Book Company,Inc, 1952.

8. Ash, Milton. *Nuclear Reactor Kinetics.* New York:McGraw-Hill Book Company,Inc, 1965.

9. Roney, James R. *A Pile Oscillator for the AGN-201 Reactor.* Monterey, California: US Naval Postgraduate School, 1959. Retrieved Nov 3 ,2013.

10. Engen, Ivar A. *A New Technique for Investigating Feedback and Stability of a Nuclear Reactor.* Argonne National Laboratory, EBR-II Project, June 1970. Retrieved Nov 13 ,2013.

11. Singh ,Om Pal and K, Obaidurrahman.*Investigation of Neutronic Decoupling Phenomenon in Large Reactors.* IIT, India, Asian Nuclear Prospects, 2010. Retrieved October, 2013.

12. Kreyszig, Erwin. *Advanced Engineering Mathmatics.* Hoboken, New Jersey : John Wiley & Sons Inc, 2006. ISBN 0471728977.

13. Dennis, Dr. Stowe. *Personal Communication.* December 8, 2013.

14. Jackson,John David. *Classical Elctrodynamics.* : John Wiley & Sons, inc., 2007.

15. Kim,Soon S. et.all. *Advanced Test Ractor:Serpentine Arrangement of Highly Enriched Water Moderated Uranium-Aluminide Fuel Plates Reflected by Beryllium.*. U.S. Department of Energy, Idaho National Laboratory, 2005.

16. Bess,John D. et.all. *FreshCore Reload of the Neutron Radiography (NRAD) Reactor with Uranium (20) –Erbium -Zirconium-Hydride Fuel* Department of Energy, Idaho National Laboratory.

17. *SCALE: A Modular Code System for Performing Standardized Computer Analyses for Licensing Evaluation*, RISC Computer Code Collection, CCC-545, NUREG/CR-0200, Rev. 4, ORNL/NUREG/CSD-2/R4, Oak Ridge National Lab.

18. L. M. Petrie and N. F. Landers, *KENO-V.a - An Improved Monte Carlo Criticality Program with Supergrouping*, NUREG/CR-0200, Oak Ridge National Laboratory, December, 1984.

19. *International Handbook of Evaluated Criticality Safety Benchmark Experiments*, NEA/NSC/DOC (95)03/I-VI, Nuclear Energy Agency, Retrieved 7th Dec, 2013.

20. Lamarsh, John, and Anthony Baratta. *Introduction to Nuclear Engineering*. 3rd Edition. Upper Saddle River: Prentice Hall, 2001. 1-759. Print.

21. Baum, Edward, Harold Knox, and Thomas Miller. *Chart of the Nuclides: Nuclides and Isotopes*. 16th Edition. 1. Schenectady: Lockheed Martin Corporation, 2002. 1-88. Print.

22. Kapusta, B., C. Sainte-Catherine, X. Averty, M. Scibetta, G.M. Decroix, and M. Rommens. "Present Status on the Mechanical Characterization of Aluminum Alloys 5754-Net-O and 6061-T6 Irradiated at High Fluences." *International Group on Research Reactors*. International Group on Research Reactors Inc., 2009. Web. 3 Dec 2013. <http://www.igorr.com/home/liblocal/docs/Proceeding /Meeting 8/sld_09.pdf>.

23. "6061-T6 Aluminum Tube." *Online Metals*. Online Metals Inc., 2012. Web. 3 December 2013. <http://www.onlinemetals.com/merchant.cfm?step=2&id=71>.

24. "Aluminum." *Wikipedia*. Wikipedia Inc., 24 December, 2013. <http://en.wikipedia.org/wiki/Aluminum>.

25. Raines, J.W. *Reactivity Measurement in a Fast Reactor by the Polarity Coherence Technique.* Pocatello : Idaho State University (Thesis), 1971.

26. Foell, Wesley. *SmallSample Reactivity Measurements in Nuclear Reactors*. Hinsdale, Illinois : American Nuclear Society, 1972.

27. MATLAB Version 7-10-0. Natick, Massachusetts: The MathWorks Inc., 2010.

28. Wolfram Research, Inc., Mathematica, Version 9.0.1, Champaign, IL, 2013.

29. MCNP , Los Alamos National Laboratory (LANL), 1957. Retrived April 2nd, 2014.

30. KENO V.a, Oak Ridge National Laboratory (ORNL), TN, 1998. Retrived April 1st ,2014.

31. LabVIEW, National Instruments, August 6th, 2013. Retrived March 1st , 2014.

APPENDICES

Derivation of Kinetic Equations

The equation of continuity is a mathematical expression that describes the balance of neutrons in a specified volume (reactor) (Lamarsh, 2001).

$$\begin{aligned} Rate\ of\ change\ in\ neutrons\ in\ volume \\ = [Rate\ of\ production\ of\ neutrons\ in\ volume] \\ - [Rate\ of\ absorption\ of\ neutrons\ in\ volume] \\ - [Rate\ of\ leakage\ of\ neutrons\ from\ volume] \end{aligned} \quad [15]$$

Each of the terms in the continuity equation is explained separately.

The total number of neutrons can be found out by integrating the neutron density throughout the volume.

$$Total\ number\ of\ neutrons = \int ndV \quad [16]$$

Where, n is the neutron density and V is the specified volume.

$$Rate\ of\ change\ in\ number\ of\ neutrons = \frac{d}{dt}\int ndV = \int \frac{\partial}{\partial t} ndV \quad [17]$$

In moving the time derivative inside the integral, it is required to change the full derivative to partial as neutron density may be a function of space as well (Lamarsh, 2001)

$$Production\ rate\ of\ neutrons\ in\ volume, V = \int sdV \quad [18]$$

Where s is the rate at which neutrons are emitted.

$$Absorption\ rate\ of\ neutrons\ in\ volume, V = \int \Sigma_a \phi\, dV \quad [19]$$

Where $\Sigma_a$the macroscopic absorption is cross section and ϕ is the neuron flux.

Not all the neutrons contribute in the chain reaction because some of them leak out of the core. The rate at which neutrons leak out of the reactor is given by the leakage rate:

$$Leakage\ rate\ of\ neutrons\ in\ volume, V = \int \boldsymbol{J}.d\boldsymbol{A} \quad [20]$$

Where, $\boldsymbol{J}$ is the neutron current density vector at the specified volume. The trick in the equation [18] is the use of the divergence theorem which converts the surface integral to the volume integral in order to compare with the volume integration of the other terms (e.g. equation 16).

The equation of continuity i.e. equation 15 can be written as:

$$\int n \frac{\partial}{\partial t} dV = \int s\, dV - \int \Sigma_a \phi\, dV - \int \boldsymbol{\Delta J} d\boldsymbol{A} \quad [21]$$

Since equation 21 contains the integration over the same volume and the volume is arbitrary so we can simplify.

Equation 21 simplifies to

$$\frac{\partial}{\partial t} n = \mathrm{s} - \Sigma_a \phi - \boldsymbol{\Delta J} \quad [22]$$

The current density ($\boldsymbol{J}$) in the equation 21 can be related to flux with the help of the Fick's law. Fick's law states:

$$\boldsymbol{J} = -\mathrm{D}\boldsymbol{\Delta}\phi \quad [23]$$

Where, D is the diffusion coefficient with the units of cm, **Δ** is the gradient operator.

From the above equations, the one speed diffusion equation can be written as:

$$\frac{1}{v}\frac{\partial \phi}{\partial \mathrm{t}} - \mathrm{D}\nabla^2\phi + \Sigma_a\phi(r,t) = S(r,t) \quad [24]$$

Where, v is the neutron speed (neutron flux/neutron density), ∇^2 is the Laplacian (div grad), and $S(r,t)$ is the total source contribution in the diffusion equation which is given as:

$$S(r,t) = (1-\beta)v\Sigma_f\phi(r,t) + \sum_{i=1}^{6}\lambda_i C_i\,(r,t) \quad [25]$$

Where, β is the delayed neutron fraction (fraction of the delayed neutrons from group "i" to total number of neutrons). The presence of the delayed neutrons is crucial in reactor control and the kinetic behavior of the reactor. These delayed neutrons fit into six groups. Σ_f is the fission cross-section, $C_i(r,t)$ is the precursors concentration, λ_i is the decay constant of the ith group.

Combining the above two equations 24 and 25, we obtain:

$$\frac{1}{v}\frac{\partial \phi}{\partial \mathrm{t}} - \mathrm{D}\nabla^2\phi + \Sigma_a\phi(r,t) = (1-\beta)v\Sigma_f\phi(r,t) + \sum_{i=1}^{6}\lambda_i C_i\,(r,t) \quad [26]$$

A similar balance equation can be written for the precursor concentration:

$$\frac{\partial C_i}{\partial t} = \beta_i v\Sigma_f\phi(r,t) - \lambda_i C_i(r,t) \quad [27]$$

Equations 26 and 27 are two differential equations describing the neutron flux in a reactor including the delayed neutron precursor.

Mathematica Input Listings

```
SetDirectory[ToFileName[{"C:", "LANL", "atr"}]];
Needs["PlotLegends`"]

newfile = Import["tally data.xls", "XLS"];
newfile = Flatten[newfile, 1];
size = Length[newfile];

x = Table[Extract[newfile, {x, 1}], {x, 1, size}];
y = Table[Extract[newfile, {x, 2}], {x, 1, size}];
flux = Table[Extract[newfile, {x, 4}], {x, 1, size}];
error = Table[Extract[newfile, {x, 5}], {x, 1, size}];


ShowLegend[ListDensityPlot[Thread[{x, y, flux}], ColorFunction → "Rainbow"],
 {ColorData["Rainbow"][1 - #1] &, 10, "1.36E-4", "7E-14", LegendPosition → {1.1, -.75}, LegendShadow → None, LegendSize → 1.6}]
```

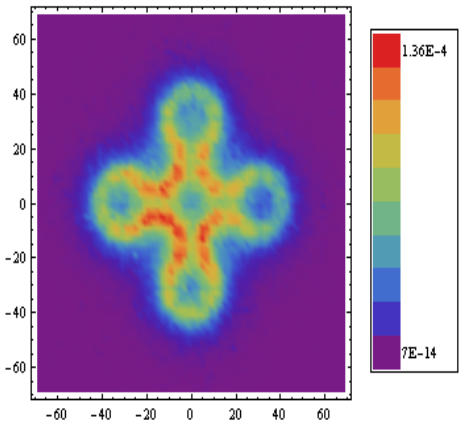

```
ListPlot3D[Thread[{x, y, flux}]]
```

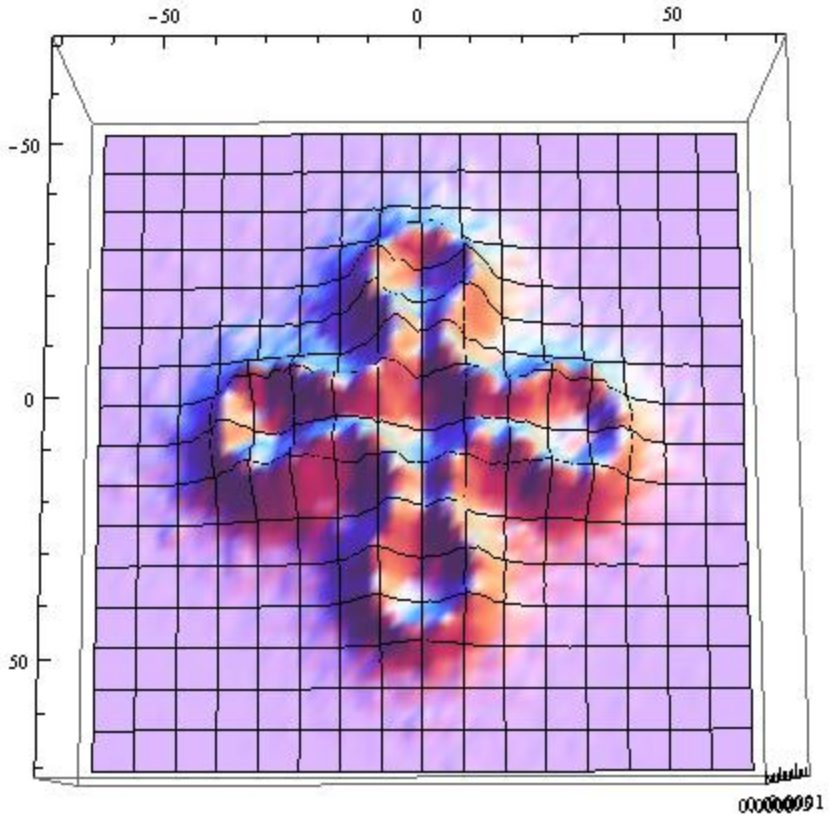

In[1]:=
```
u = x / 50;
v = y / 50;
flux = (u^4 - 6*u^2*v^2 + v^4)^2 + (4*u*v (u - v))^2
```

Out[3]=
$$\frac{x^2 \left(\frac{x}{50} - \frac{y}{50}\right)^2 y^2}{390\,625} + \left(\frac{x^4}{6\,250\,000} - \frac{3\,x^2\,y^2}{3\,125\,000} + \frac{y^4}{6\,250\,000}\right)^2$$

In[4]:=
```
FluxRectangular = -0.30250000000000005` + x^2 (x/50 - y/50)^2 y^2 / 390625 + (-0.45` + x^4/6250000 - 3 x^2 y^2/3125000 + y^4/6250000)^2;
ContourPlot[FluxRectangular, {x, -70, 70}, {y, -70, 70}, PlotRange → Full]
```

Out[5]=

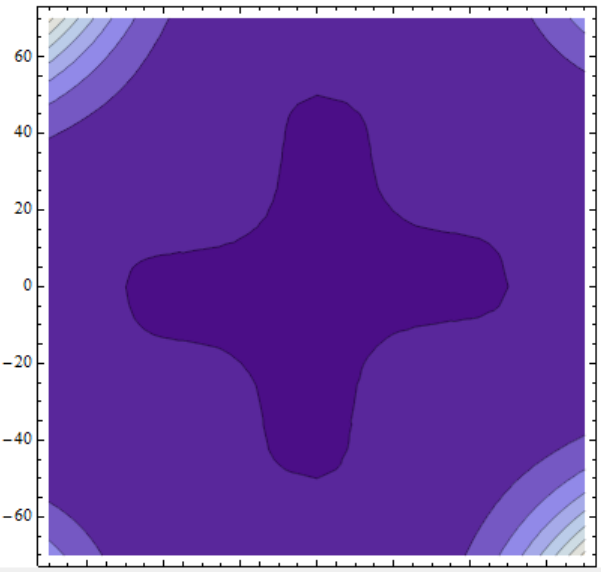

```
x = r Cos[θ];
y = r Sin[θ];
```

$$\text{FluxSpherical} = -0.30250000000000005` + \frac{x^2 \left(\frac{x}{50} - \frac{y}{50}\right)^2 y^2}{390\,625} + \left(-0.45` + \frac{x^4}{6\,250\,000} - \frac{3\,x^2\,y^2}{3\,125\,000} + \frac{y^4}{6\,250\,000}\right)^2$$

$$-0.3025 + \frac{r^4 \text{Cos}[\theta]^2 \text{Sin}[\theta]^2 \left(\frac{1}{50} r \text{Cos}[\theta] - \frac{1}{50} r \text{Sin}[\theta]\right)^2}{390\,625} + \left(-0.45 + \frac{r^4 \text{Cos}[\theta]^4}{6\,250\,000} - \frac{3\,r^4 \text{Cos}[\theta]^2 \text{Sin}[\theta]^2}{3\,125\,000} + \frac{r^4 \text{Sin}[\theta]^4}{6\,250\,000}\right)^2$$

Spherical Harmonics of few "l" and "m" with Phi =90 degree, flux(r,Theta) Polar Coordinate System

```
l = 0;
m = 0;

Ylm = Sqrt[((2 * l + 1) / (4 * Pi)) * ((l - m) ! / (l + m) !) * LegendreP[l, μ]]
```

$$\frac{1}{2\sqrt{\pi}}$$

```
A00 = Abs[Integrate[1/(2 Sqrt[π]) * FluxSpherical, {r, 0, 100}, {θ, 0, 2 * Pi}]]
```

```
5744.16

l = 1;
m = 1;
Y11 = -Sqrt[3 / (8 * Pi)] * Sin[θ];
A11 = Integrate[Y11 * FluxSpherical, {r, 0, 100}, {θ, 0, 2 * Pi}]

0
```

```
l = 1;
m = 0;
Y10 = Sqrt[3 / (4 * Pi)] * Cos[θ];
A10 = Integrate[Y10 * FluxSpherical, {r, 0, 100}, {θ, 0, 2 * Pi}]
```

```
0
```

```
l = 2;
m = 2;
Y22 = 1 / 4 * Sqrt[15 / (2 * Pi)] * (Sin[θ]) ^ 2;
A22 = Integrate[Y10 * FluxSpherical, {r, 0, 100}, {θ, 0, 2 * Pi}]
```

```
0
```

```
l = 2;
m = 1;
Y21 = -Sqrt[15 / (8 * Pi)] * (Sin[θ] * Cos[θ]);
A21 = Abs[Integrate[Y21 * FluxSpherical, {r, 0, 100}, {θ, 0, 2 * Pi}]]
```

```
3328.5
```

```
l = 2;
m = 0;
Y20 = Sqrt[5 / (4 * Pi)] * (1.5 * (Cos[θ]) ^ 2 - 1 / 2);
A20 = Abs[Integrate[Y20 * FluxSpherical, {r, 0, 100}, {θ, 0, 2 * Pi}]]
```

```
3211.08
```

```
l = 3;
m = 3;
Y33 = -1 / 4 * Sqrt[35 / (4 * Pi)] * (Sin[θ]) ^ 3;
A33 = Integrate[Y33 * FluxSpherical, {r, 0, 100}, {θ, 0, 2 * Pi}]
```

```
0
```

```
l = 3;
m = 2;
Y32 = 1 / 4 * Sqrt[105 / (2 * Pi)] * (Sin[θ]) ^ 2 * Cos[θ];
A32 = Integrate[Y32 * FluxSpherical, {r, 0, 100}, {θ, 0, 2 * Pi}]
```

```
0
```

```
l = 3;
m = 1;
Y31 = -1 / 4 * Sqrt[21 / (4 * Pi)] * Sin[θ] * (5 * (Cos[θ]) ^ 2 - 1);
A31 = Integrate[Y31 * FluxSpherical, {r, 0, 100}, {θ, 0, 2 * Pi}]
```

```
0
```

```
l = 3;
m = 0;
Y30 = Sqrt[7 / (4 * Pi)] * (5 / 2 * (Cos[θ]) ^ 3 - 3 / 2 * (Cos[θ]));
A30 = Abs[Integrate[Y30 * FluxSpherical, {r, 0, 100}, {θ, 0, 2 * Pi}]]
```

```
0.000023883
```

General Ylm when m =0

```
Y40 = Sqrt[((2 * l + 1) / (4 * Pi))] * LegendreP[l, μ] /. l → 4 /. μ → Cos[θ];

A40 = Abs[Integrate[Y40 * FluxSpherical, {r, 0, 100}, {θ, 0, 2 * Pi}]]
```

12 696.9

```
Y50 = Sqrt[((2 * l + 1) / (4 * Pi))] * LegendreP[l, μ] /. l → 5 /. μ → Cos[θ];

A50 = Abs[Integrate[Y50 * FluxSpherical, {r, 0, 100}, {θ, 0, 2 * Pi}]]
```

0

```
Y60 = Sqrt[((2 * l + 1) / (4 * Pi))] * LegendreP[l, μ] /. l → 6 /. μ → Cos[θ];

A60 = Abs[Integrate[Y60 * FluxSpherical, {r, 0, 100}, {θ, 0, 2 * Pi}]]
```

9546.82

```
Y70 = Sqrt[((2 * l + 1) / (4 * Pi))] * LegendreP[l, μ] /. l → 7 /. μ → Cos[θ];

A70 = Abs[Integrate[Y70 * FluxSpherical, {r, 0, 100}, {θ, 0, 2 * Pi}]]
```

0

```
Y80 = Sqrt[((2 * l + 1) / (4 * Pi))] * LegendreP[l, μ] /. l → 8 /. μ → Cos[θ];

A80 = Abs[Integrate[Y80 * FluxSpherical, {r, 0, 100}, {θ, 0, 2 * Pi}]]
```

7740.09

```
Y90 = Sqrt[((2 * l + 1) / (4 * Pi))] * LegendreP[l, μ] /. l → 9 /. μ → Cos[θ];

A90 = Abs[Integrate[Y90 * FluxSpherical, {r, 0, 100}, {θ, 0, 2 * Pi}]]

0

Y10 = Sqrt[((2 * l + 1) / (4 * Pi))] * LegendreP[l, μ] /. l → 10 /. μ → Cos[θ];

A100 = Abs[Integrate[Y10 * FluxSpherical, {r, 0, 100}, {θ, 0, 2 * Pi}]]

6605.03

Y11 = Sqrt[((2 * l + 1) / (4 * Pi))] * LegendreP[l, μ] /. l → 11 /. μ → Cos[θ];

A110 = Abs[Integrate[Y11 * FluxSpherical, {r, 0, 100}, {θ, 0, 2 * Pi}]]

0

Clear [x, y]|

x = x
y = y

x

y
```

$$\text{FluxRectangularr} = -0.30250000000000005 + \frac{x^2 \left(\frac{x}{50} - \frac{y}{50}\right)^2 y^2}{390\,625} + \left(-0.45` + \frac{x^4}{6\,250\,000} - \frac{3\,x^2\,y^2}{3\,125\,000} + \frac{y^4}{6\,250\,000}\right)^2$$

$$-0.3025 + \frac{x^2 \left(\frac{x}{50} - \frac{y}{50}\right)^2 y^2}{390\,625} + \left(-0.45 + \frac{x^4}{6\,250\,000} - \frac{3\,x^2\,y^2}{3\,125\,000} + \frac{y^4}{6\,250\,000}\right)^2$$

```
FluxProfile = (A00 * FluxRectangularr + A11 * FluxRectangularr + A10 * FluxRectangularr + A22 * FluxRectangularr + A20 * FluxRectangularr +
    A33 * FluxRectangularr + A31 * FluxRectangularr + A30 * FluxRectangularr + A40 * FluxRectangularr + A50 * FluxRectangularr + A60 * FluxRectangular
    A70 * FluxRectangularr + A80 * FluxRectangularr + A90 * FluxRectangularr + A100 * FluxRectangularr + A110 * FluxRectangularr)
```

$$45544.1 \left(-0.3025 + \frac{x^2 \left(\frac{x}{50} - \frac{y}{50}\right)^2 y^2}{390\,625} + \left(-0.45 + \frac{x^4}{6\,250\,000} - \frac{3\,x^2\,y^2}{3\,125\,000} + \frac{y^4}{6\,250\,000}\right)^2\right)$$

```
ContourPlot[FluxProfile, {x, -70, 70}, {y, -70, 70}, PlotRange → Full]
```

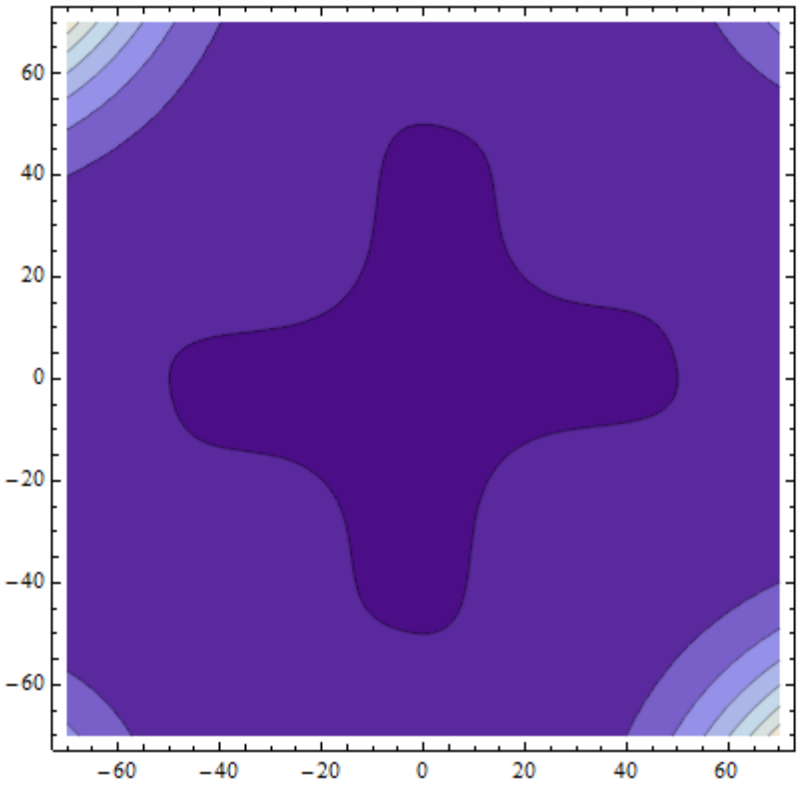

MATLAB File to Get the Transfer Function of NRAD

```
function [ D phase] = AGNTransferFunction( freq,rho,version)
%AGNTRANSFERFUNCTION Calculates the magnitude of the transfer function
at a
%specified frequency
%


if isempty(version)
    disp('Warning you did not chose a version of parameters!!!')
   version = 1;
end


if version == 1
    % 1st Old version of parameters
    Beta=0.00745;
    % Duderstadt estimates
    Betaj=[0.038 0.213 0.188 0.407 0.128 0.026]*Beta;
    Lambdaj=[1/55.79, 1/22.78, 1/6.33, 1/2.18, 1/0.512, 1/0.08]*log(2);
    Gen_Life = 62.2E-6;


elseif version == 2
    % 2nd Old version of parameters
    Beta=0.00745;
    Betaj=[0.038 0.213 0.188 0.407 0.128 0.026]*Beta;
    Lambdaj=[1/55.72, 1/22.72, 1/6.22, 1/2.3, 1/0.610, 1/0.23]*log(2);
    Gen_Life = 62.2E-6;
```

```
elseif version == 3
    % Data from fit of Transfer Function 2013
    Lambdaj = [0.0135261,0.0296958,0.114594,0.299206,1.04434,5.43916];
    Betaj=[0.000283,0.001563,0.001835,0.002259,0.001183,0.000343];
    Beta = sum(Betaj);
    Gen_Life = 62.2E-6;

elseif version == 4
    % MCNP
    Beta=0.00745;
    Betaj = [0.03183 0.1657 0.1644 0.4575 0.1339 0.0464]*Beta;
    Lambdaj=[1/55.49365, 1/21.78519, 1/6.33547, 1/2.18564, 1/0.51208,
1/0.08016]*log(2);
    Gen_Life = 62.2E-6;
elseif version == 5
    % Very Old Parameters
    Betaj=[0.00024,0.00163, 0.00147, 0.00295, 0.00074, 0.00031];
    Lambdaj=[1/55.72, 1/22.72, 1/6.22, 1/2.3, 1/0.610, 1/0.23]*log(2);
    Beta=0.00734;
    Gen_Life = 7.499*10^(-5);

elseif version == 6
    %NO idea where this came from

Betaj=[0.00028309,0.00156321,0.00183519,0.00225935,0.00118252,0.0003433
74];
    Lambdaj=[0.0135261,0.0296958,0.114594,0.299206,1.04434,5.43916];
    Gen_Life = 5.96103E-5;
```

```
elseif version == 7
    % 1st Old version of parameters and NRAD Parameters
    Beta=0.0075;
    % Duderstadt paramers
    Betaj=[0.038 0.213 0.188 0.407 0.128 0.026]*Beta;
    Lambdaj=[1/54.51, 1/21.84, 1/6.00, 1/2.23, 1/0.496,
1/0.179]*log(2);
    Gen_Life = 24.5E-6;


end



G = zeros(1,length(freq));
sums = 0;
for jj = 1:length(freq)
    for ii = 1:6
        sums = sums + Betaj(ii)/(Lambdaj(ii)+1i*2*pi*freq(jj));
    end


    G(jj) = 1/((1i*2*pi*freq(jj)*(Gen_Life+sums))-rho);
    sums = 0;
end
D = abs(G);
phase = angle(G);
end
```

Input Listing of KENO-3D of NRAD

```
'Input generated by GeeWiz SCALE 6.1 Compiled on  Feb 6
11:04:33 2014
=csas6
fresh-core reload of the nrad reactor with u(20)-er-zr-h
fuel (simple)
v7-238
read composition
 c-graphite  1 0 0.078692 294   end
 h-zrh2      3 0 0.050608 294   end
 b           3 0 4.1524e-07 294
                                5010 19.9
                                5011 80.1   end
 c           3 0 0.0010781 294   end
 zr-zrh2     3 0 0.03203 294   end
 er          3 0 0.00023226 294
                                68162 0.14
                                68164 1.61
                                68166 33.61
                                68167 22.93
                                68168 26.78
                                68170 14.93   end
 hafnium     3 0 1.9297e-06 294
                                72174 0.16
```

```
                                72176 5.26
                                72177 18.6
                                72178 27.28
                                72179 13.62
                                72180 35.08   end
u-234       3 0 1.1036e-05 294   end
u-235       3 0 0.0010844 294   end
u-236       3 0 1.0942e-05 294   end
u-238       3 0 0.0043326 294   end
c-graphite  4 0 0.086734 294   end
mo          5 0 0.06413 294
                                42092 14.84
                                42094 9.25
                                42095 15.92
                                42096 16.68
                                42097 9.55
                                42098 24.13
                                42100 9.63   end
zirconium   6 0 0.042897 294
                                40090 51.45
                                40091 11.22
                                40092 17.15
                                40094 17.38
                                40096 2.8   end
```

```
c           7 0 0.00016044 294   end
si          7 0 0.00068614 294
                                 14028 92.2297
                                 14029 4.6832
                                 14030 3.0871   end
p           7 0 4.0441e-05 294   end
s           7 0 3.3049e-06 294
                                 16032 94.93
                                 16033 0.76
                                 16034 4.29
                                 16036 0.02   end
cr          7 0 0.017604 294
                                 24050 4.345
                                 24052 83.789
                                 24053 9.501
                                 24054 2.365   end
mn          7 0 0.00087693 294   end
fe          7 0 0.059271 294
                                 26054 5.845
                                 26056 91.754
                                 26057 2.119
                                 26058 0.282   end
ni          7 0 0.0082087 294
                                 28058 68.0769
```

```
                                    28060 26.2231
                                    28061 1.1399
                                    28062 3.6345
                                    28064 0.9256   end
 b-10          8 0 0.021515 294   end
 b-11          8 0 0.086601 294   end
 c-graphite    8 0 0.027029 294   end
 al            9 0 0.058953 294   end
 h             10 0 0.066619 294   end
 o             10 0 0.033309 294   end
end composition
read celldata
  latticecell squarepitch fuelr=1.74025 3 gapr=1.7447 0
cladr=1.7955 7 hpitch=1.97612 10 end
end celldata
read parameter
 gen=1550
 npg=100000
 nsk=50
 htm=yes
end parameter
read geometry
unit 1
com="graphite reflector block"
```

```
 cuboid 1    3.683   -3.683    3.683   -3.683  65.72251
0
 cuboid 2  4.535029  -4.535029  4.535029  -4.535029
65.72251        0   rotate  a1=45 a2=0 a3=0
 cuboid 3  4.05003  -4.05003  3.85445  -3.85445      120
-19.92
 media 1 1 1 2
 media 10 1 -1 2
 media 10 1 -2 3
 boundary 3
unit 2
com="fuel rod"
 cylinder 1   1.7955  63.81751     5.08
 cylinder 2   1.7447  63.81751     5.08
 cylinder 3  1.63957  15.0368     6.35
 cylinder 4  1.73482  15.11618  15.0368
 cylinder 5  0.28575  53.13618  15.11618
 cylinder 6  1.74025  53.13618  15.11618
 cylinder 7    0.316  53.13618  15.11618
 cylinder 8  1.63957  61.82298  53.13618
 cylinder 9   1.7447     6.35     5.08
 cylinder 10   1.7447  62.54751  61.82298
 cylinder 11   1.7447  63.81751  62.54751
```

```
 cuboid 12   1.9431  -1.9431   1.9431  -1.9431      120   -
19.92
 media 7 1 1 -2
 media 7 1 9
 media 4 1 3
 media 6 1 5
 media 0 1 -5 7
 media 3 1 6 -7
 media 4 1 8
 media 7 1 11
 media 0 1 2 -3 -4 -6 -8 -9 -11
 media 10 1 -1 12
 media 5 1 4
 boundary 12
unit 6
com="all fuel rods"
 cuboid 1  4.05003  -4.05003  3.85445  -3.85445      120
-19.92
 array 1 1  place 2 2 1 -1.9431 -1.9431 0
 boundary 1
unit 7
com="water"
 cuboid 1  4.05003  -4.05003  3.85445  -3.85445      120
-19.92
```

```
 media 10 1 1
 boundary 1
global unit 8
com="tank"
 cylinder 1       45      120   -19.92
 cuboid 2       45  17.92069    6.985   -6.985  42.38117
25.78118
 cuboid 4    6.985   -6.985       45  17.33395  42.38117
25.87118
 array 2 1 -2 -4  place 6 6 1 -4.05003 -3.85445 0
 media 0 1 1 2
 media 0 1 4 1
 boundary 1
unit 3
com="water smaller unit"
 cuboid 1   1.9431  -1.9431   1.9431  -1.9431      120   -
19.92
 media 10 1 1
 boundary 1
unit 9
com="shim"
 cylinder 1  1.51638    53.34  51.7525
 cylinder 2  1.50749    91.44    53.34
 cylinder 3  1.51638  111.1885   109.22
```

```
 cylinder 4  1.51638  111.1885  51.7525
 cylinder 5   1.5875  111.1885  51.7525
 cuboid 6   1.9431  -1.9431   1.9431  -1.9431      120   -
19.92
 media 9 1 5 -4
 media 9 1 1
 media 8 1 2
 media 9 1 3
 media 0 1 4 -1 -2 -3
 media 10 1 6 -5
 boundary 6
unit 10
com="reg"
 cylinder 1  1.51638  35.6616  34.0741
 cylinder 2  1.50749  73.7616  35.6616
 cylinder 3  1.51638  93.5101  91.5416
 cylinder 4  1.51638  93.5101  34.0741
 cylinder 5   1.5875  93.5101  34.0741
 cuboid 6   1.9431  -1.9431   1.9431  -1.9431      120   -
19.92
 media 9 1 5 -4
 media 9 1 1
 media 8 1 2
 media 9 1 3
```

```
 media 0 1 4 -1 -2 -3
 media 10 1 6 -5
 boundary 6
unit 11
com="shim 2 cluster"
 cuboid 1  4.05003  -4.05003  3.85445  -3.85445      120
-19.92
 array 3 1  place 2 2 1 -1.9431 -1.9431 0
 boundary 1
unit 12
com="shim 1 cluster"
 cuboid 1  4.05003  -4.05003  3.85445  -3.85445      120
-19.92
 array 4 1  place 2 2 1 -1.9431 -1.9431 0
 boundary 1
unit 13
com="reg rod cluster"
 cuboid 1  4.05003  -4.05003  3.85445  -3.85445      120
-19.92
 array 5 1  place 2 2 1 -1.9431 -1.9431 0
 boundary 1
unit 14
com="three rod cluster"
```

```
 cuboid 1  4.05003  -4.05003  3.85445  -3.85445      120
-19.92
 array 6 1  place 2 2 1 -1.9431 -1.9431 0
 boundary 1
end geometry
read array
ara=1 nux=4 nuy=4 nuz=1 typ=square
 com=''
 fill
    3    3    3    3
    3    2    2    3
    3    2    2    3
    3    3    3    3  end fill
ara=2 nux=12 nuy=12 nuz=1 typ=square gbl=2
 com=''
 fill
    7    7    7    7    7    7    7    7    7    7    7
7
    7    7    7    7    7    7    7    7    7    7    7
7
    7    7    7    7    7    7    7    7    7    7    7
7
    7    7    7    7    1    1    1    1    7    7    7
7
```

```
    7    7    7    1    6    6    6    6    1    7    7
7
    7    7    7    1   12    6    6    6    7    7    7
7
    7    7    7    1   11    6   14    6    7    7    7
7
    7    7    7    1    6    6    6    6    1    7    7
7
    7    7    7    7    1    7    7    1    7    7    7
7
    7    7    7    7    7    7    7    7    7    7    7
7
    7    7    7    7    7    7    7    7    7    7    7
7
    7    7    7    7    7    7    7    7    7    7    7
7  end fill
ara=3 nux=4 nuy=4 nuz=1 typ=square
 com='shim rod 2'
 fill
    3    3    3    3
    3    2    2    3
    3    2    9    3
    3    3    3    3  end fill
ara=4 nux=4 nuy=4 nuz=1 typ=square
```

```
 com=''
 fill
    3    3    3    3
    3    2    9    3
    3    2    2    3
    3    3    3    3  end fill
ara=5 nux=4 nuy=4 nuz=1 typ=square
 com='reg rod cluster'
 fill
    3    3    3    3
    3    2    2    3
    3    2   10    3
    3    3    3    3  end fill
ara=6 nux=4 nuy=4 nuz=1 typ=square
 com='three rod cluster'
 fill
    3    3    3    3
    3    3    2    3
    3    2    2    3
    3    3    3    3  end fill
end array
read plot
 scr=yes
 ttl='x-y plot'
```

```
 pic=mixtures
 xul=-45
 yul=0
 zul=120
 xlr=45
 ylr=0
 zlr=-19.92
 nax=800
 clr=1 255 0 0
     3 0 229 238
     4 0 238 0
     5 205 205 0
     6 238 0 0
     7 145 44 238
     8 150 150 150
     9 240 200 220
     10 0 191 255
 end color
 uax=1 wdn=-1
  end
end plot
end data
end
```

IEU-MET-FAST-010 Benchmark to Validate KENO

KENO 238-Group Input Listing, Table 29.a.

```
=csas25 parm=size=1000000
IEU-MET FAST-010
238gr infh
' core 1
u-235 1 0 3.48543-3 end
u-238 1 0 3.52634-2 end
u-234 1 0 3.34211-5 end
u-236 1 0 1.60227-5 end
cr 1 0 1.86067-3 end
ni 1 0 7.49053-4 end
fe 1 0 6.65688-3 end
c 1 0 9.62990-5 end
mo 1 0 1.18327-5 end
mn 1 0 1.63509-4 end
cu 1 0 2.38833-5 end
h 1 0 1.94580-5 end
si 1 0 7.16001-5 end
cl 1 0 3.33506-5 end
f 1 0 9.91220-5 end
' core 2
u-235 2 0 3.47666-3 end
u-238 2 0 3.53869-2 end
u-234 2 0 3.33328-5 end
u-236 2 0 1.59801-5 end
cr 2 0 1.87418-3 end
ni 2 0 7.54654-4 end
fe 2 0 6.70752-3 end
c 2 0 9.64166-5 end
mo 2 0 1.19799-5 end
mn 2 0 1.64823-4 end
cu 2 0 2.42329-5 end
h 2 0 1.94498-5 end
si 2 0 7.42038-5 end
cl 2 0 3.34686-5 end
f 2 0 9.94726-5 end
' core 3
u-235 3 0 3.48543-3 end
u-238 3 0 3.52634-2 end
u-234 3 0 3.34211-5 end
u-236 3 0 1.60227-5 end
cr 3 0 1.86067-3 end
ni 3 0 7.49053-4 end
fe 3 0 6.65688-3 end
c 3 0 9.62606-5 end
mo 3 0 1.18327-5 end
mn 3 0 1.63509-4 end
cu 3 0 2.38833-5 end
h 3 0 1.94471-5 end
si 3 0 7.16001-5 end
cl 3 0 3.33314-5 end
f 3 0 9.90650-5 end
' core 4
u-235 4 0 3.47666-3 end
u-238 4 0 3.53869-2 end
u-234 4 0 3.33328-5 end
u-236 4 0 1.59801-5 end
cr 4 0 1.87418-3 end
ni 4 0 7.54654-4 end
fe 4 0 6.70752-3 end
c 4 0 9.63781-5 end
```

KENO 238-Group Input Listing, Table 29.a (cont'd).

```
mo 4 0 1.19799-5 end
mn 4 0 1.64823-4 end
cu 4 0 2.42329-5 end
```

KENO 238-Group Input Listing, Table 29.a (cont'd).

h 4 0 1.94388-5 end
si 4 0 7.42038-5 end
cl 4 0 3.34493-5 end
f 4 0 9.94154-5 end
' upper DU axial reflector
u-235 5 0 8.31425-5 end
u-238 5 0 3.72293-2 end
cr 5 0 1.72627-3 end
ni 5 0 7.03836-4 end
fe 5 0 6.26656-3 end
al 5 0 4.16747-4 end
c 5 0 3.99149-5 end
mo 5 0 1.12206-5 end
mn 5 0 1.46859-4 end
cu 5 0 2.13537-5 end
h 5 0 2.85427-6 end
si 5 0 8.31237-5 end
cl 5 0 4.93394-6 end
f 5 0 1.46107-5 end
' lower DU axial reflector
u-235 6 0 8.24312-5 end
u-238 6 0 3.69113-2 end
cr 6 0 1.72627-3 end
ni 6 0 7.03836-4 end
fe 6 0 6.26607-3 end
al 6 0 4.16747-4 end
c 6 0 3.97675-5 end
mo 6 0 1.12206-5 end
mn 6 0 1.46859-4 end
cu 6 0 2.13537-5 end
h 6 0 2.81777-6 end
si 6 0 8.31237-5 end
cl 6 0 4.87118-6 end
f 6 0 1.44249-5 end
' DU radial reflector
u-235 7 0 8.56868-5 end
u-238 7 0 3.83747-2 end
cr 7 0 1.69502-3 end
ni 7 0 6.86302-4 end
fe 7 0 6.13244-3 end
c 7 0 3.77935-5 end
mo 7 0 1.07671-5 end
mn 7 0 1.46803-4 end
cu 7 0 2.16820-5 end
h 7 0 2.53803-6 end
si 7 0 7.69676-5 end
cl 7 0 4.39454-6 end
f 7 0 1.30132-5 end
' empty mATR-Cix above and below reflector
cr 8 0 1.18901-3 end
ni 8 0 4.80175-4 end
fe 8 0 4.27914-3 end
c 8 0 1.87415-5 end
mo 8 0 8.25653-6 end
mn 8 0 1.05905-4 end
cu 8 0 1.72319-5 end
si 8 0 6.83105-5 end
' empty mATR-Cix beyond radial rfelector
cr 9 0 1.17957-3 end
ni 9 0 4.76329-4 end
fe 9 0 4.24488-3 end
c 9 0 1.85933-5 end
mo 9 0 8.19076-6 end
mn 9 0 1.05057-4 end
cu 9 0 1.70944-5 end

KENO 238-Group Input Listing, Table 29.a (cont'd).
si 9 0 6.77630-5 end
end comp
IEU-MET-FAST-010

```
read geom
unit 1
cyli 1 1 40.996 22.941 0.000
cyli 2 1 40.996 38.181 0.000
cyli 3 1 40.996 38.181 -22.941
cyli 4 1 40.996 38.181 -38.181
cyli 5 1 40.996 120.461 -38.181
cyli 6 1 40.996 120.461 -120.461
cyli 8 1 40.996 120.975 -120.975
cyli 7 1 65.159 120.975 -120.975
cyli 8 1 65.159 121.920 -121.920
cyli 9 1 96.623 121.920 -121.920
end geom
read start nst=1
xsp=50 xsm=-50 ysp=50 ysm=-50 zsp=50 zsm=-50
end start
end data
end
```

KENO-V.a- Final Results

Keno-V.a - Final Results
term paper

Best Estimate System k_{eff}	0.9901 ± 0.0016
Energy of Average Lethargy of Fission (eV)	3.65492E+005 ± 1.81662E+003
System $\bar{\nu}$	2.55590E+000 ± 6.73251E-004
System Mean Free Path (cm)	2.48235E+000 ± 2.71071E-003
Number of Warning Messages	41
Number of Error Messages	0
k_{eff} satisfies the χ^2 for normality at the 95 % level	

Congratulations! You have successfully traversed the perilous path through Keno-V.a in 17.08667 minutes